공학박사 학위논문

A Study on Protein Fouling and Virus Breakthrough Phenomena of Virus Filtration Membrane in Biopharmaceutical Downstream Process

항체의약품 정제용 바이러스 분리막의 단백질 막 오염과 바이러스 투과 현상에 관한 연구

2023년 8월

서울대학교 대학원

화학생물 공학부

서 동 우

A Study on Protein Fouling and Virus Breakthrough Phenomena of Virus Filtration Membrane in Biopharmaceutical Downstream Process

항체의약품 정제용 바이러스 분리막의 단백질 막 오염과
바이러스 투과 현상에 관한 연구

지도교수 이 창 하

이 논문을 공학박사 학위논문으로 제출함

2023년 07월

서울대학교 대학원

공과대학 화학생물공학부

서 동 우

서동우의 공학박사 학위논문을 인준함

2023년 06월

위 원 장	윤 제 용	(인)
부위원장	이 창 하	(인)
위 원	유 동 원	(인)
위 원	조 영 훈	(인)
위 원	백 영 빈	(인)

A Study on Protein Fouling and Virus Breakthrough Phenomena of Virus Filtration Membrane in Biopharmaceutical Downstream Process

by

Dongwoo Suh

under the supervision of

Professor Changha Lee, Ph. D.

A dissertation submitted in partial fulfillment of the requirements for the Degree of Doctor of Philosophy

August 2023

SCHOOL OF CHEMICL AND BIOLOGICAL ENGINEERING

SEOUL NATIONAL UNIVERSITY

Abstract

A study on Protein Fouling and Virus Breakthrough Phenomena of Virus Filtration Membrane in Biopharmaceutical Downstream Process

Dongwoo Suh

School of Chemical and Biological Engineering

The Graduates School

Seoul National University

Biopharmaceuticals are medicines based on biological sources, such as plants and animals. Biopharmaceutical manufacturing industry is rapidly growing due to the increase demand of bio-inspired medicines, such as therapeutic proteins and vaccines. However, mammalian cell-derived biopharmaceutical products are exposed to potential risk of viral contamination from adventitious or endogenous viruses. To ensure safety of biopharmaceutical products, all mammalian-cell based bio-products are required to validate viral safety from its raw material to the final product form. Therefore, biopharmaceutical manufacturing process includes viral clearance operations, such as low pH virus inactivation and virus filtration.

Virus filtration process is considered as key unit operation for viral clearance due to its robust virus removal performance and low adverse impact on bioproducts. The virus filtration is size based removal process, where virus is removed in membrane via size similarity between virus size and nominal pore size of the membrane, while biopharmaceuticals transmitted through membrane. Current virus filtration process guarantees 4-$\log_{10}$ reduction of known or unknown viruses with

over 95% of biopharmaceutical transmission. Despite the process robustness, virus filtration is suffered from severe protein fouling and undesired virus breakthrough, caused product loss, and threatening the safety of biopharmaceutical products. This dissertation investigated the two major limitations of virus filtration process, focused on membrane properties and operational conditions on process performances.

First, comprehensive evaluations were conducted by using seven different commercially available virus filtration membranes for biopharmaceutical downstream process. The unique structure of each membrane varied virus filtration performance in terms of protein fouling propensity and virus breakthrough. For protein fouling propensity, higher O/C ratio on membrane surface, larger pore existence (over 1 μm) on upper region, and 'shallow' pore size gradient of 4 – 8 nm/μm in virus retentive region caused mitigating filtrate flux decline by protein fouling up to 66.3%. The pore size distribution via gas-liquid porometry (GLP) analysis revealed pore size detection over 25 nm caused undesired virus breakthrough. The main results suggested important parameters for high performance virus filtration membrane design.

Second, virus breakthrough points under different feed solution compositions and operational conditions were investigated to determine optimal operation of virus filtration. The study revealed virus breakthrough point when virus challenge over 10^{12} PFU/m^2, in convective-force dominant batch filtration process. Low flux filtration for continuous bioprocess, however, showed early virus detection at 10^{11} PFU/m^2 due to increase the Brownian motion of virus in the membrane. Based on the experimental results, safe virus filtration operation was determined as 10^{10} PFU/m^2 of virus challenged under both batch and continuous processes.

The main results of this study give practical insights to biopharmaceutical industry and virus filtration membrane R&D industry, as the study suggested appropriate membrane selection for target biopharmaceutical with product-safety guaranteed operation limit, as well as important parameters to consider design next-generation virus filtration membrane.

Keywords: Biopharmaceuticals; Downstream process; Virus filtration; Protein fouling; Virus breakthrough

Student Number: 2014-30293

Table of Contents

List of Figures

List of Tables

1. Introduction

1.1. Research Background

The biopharmaceutical refers medicines driven from bio-resources, such as animal and plants. Biopharmaceutical manufacturing industry is rapidly growing, as 8 of the top 10 bet-selling drugs are bio-inspired medicines (Zydney, 2021). Especially, the covid-19 pandemic had resulted gaining the interest of biopharmaceuticals such as vaccines and monoclonal antibodies for prevention of the virus infection and potential cure of the disease (Ahmed Bouzidi, 2021). Also, development of manufacturing processes has enabled the mass production of biopharmaceuticals, resulted the fast market growing.

Biopharmaceutical manufacturing processes are divided into two major streams, upstream process for cell cultivation and harvesting, and downstream for purification and formulation of raw materials to form of biopharmaceuticals. Despite rapid increase of the industry, biopharmaceutical products are often exposed to risk of viral contamination by mammalian-cell derived products. Although the events of viral contaminations have rarely occurred, less than 30 events over 3 decades. However, the sources of viral contamination were broad from raw material to final product (Barone et al., 2020). Therefore, to ensure viral safety of biopharmaceutical products, International Conference on Harmonization (ICH) established a world-wide standard for viral safety “Q5A: Viral Safety Evaluation of Biotechnology Products Derived from Cell Lines of Human or Animal Origin” (ICH, 2022). The regulation requires vial safety assurance of raw material, removing or inactivating of detected virus before the final production, and the virus infective assay of final products. Among the viral safety regulations,

validation of viral clearance capability is performed during downstream process, applying two or more orthogonal processes (Zydney, 2016).

There are several virus clearance methods applied in downstream process, including low pH inactivation, chemical solvent/detergent treatment, virus removal during chromatography, and virus retentive filters (Shukla & Aranha, 2015). Among these processes, virus filtration process is considered robust virus removal process due to its high removal performance and low impact on biopharmaceutical products (Ajayi, Johnson, Faison, Azer, Cullinan, et al., 2022). Therefore, virus filtration process is widely used in both therapeutic protein purification and plasma-based products industries (Johnson et al., 2022).

The virus removal mechanism of virus filtration process is size-exclusion mechanism, where virus is effectively retained in membrane, similar as depth filtration process (Nejatishahidein & Zydney, 2021). Virus filtration membranes were divided as large-virus removal filters and small-virus removal filters, nominal pore size of 50 and 20 nm, respectively. Currently, most of downstream processes are adopted small-virus removal filters due to effective removal process of both large and small viruses by small-virus removal filters (Marques et al., 2009). The main hurdle of virus filtration process is the selective removal performance of virus due to the size similarity between small virus (18 – 26 nm) and biopharmaceuticals (8 – 10 nm) (Fallahianbijan et al., 2019). Therefore, the virus retentive membrane must have narrower pore size distribution (PSD) than ultrafiltration (UF) and microfiltration (MF) membranes to achieve selective removal of virus with high protein transmission (Goodrich et al., 2020). The tight PSD membrane characteristic of virus filtration requires high-end technology of membrane fabrication, caused high cost among other membranes used in biopharmaceutical

downstream process (Barnard et al., 2014).

Currently, single virus filtration process provides over 95% of product yield with >99.99% (4-$\log_{10}$ reduction) of target virus removal performance (Zydney, 2016). However, virus filtration process is still limited by two major phenomena: protein fouling and virus breakthrough during virus filtration process. Protein fouling defined as undesired protein deposition or clogging on virus filtration membrane, caused decreasing flow rate and lower product yields. Undesired virus breakthrough is the migration of virus through virus filtration membrane by various complication of virus filtration, caused product safety fail, require additional virus clearance method to ensure product safety. Previous studies accomplished to define the mechanisms of protein fouling and undesired virus breakthrough in various aspects, the quantitative analysis for protein fouling and virus breakthrough were still limited by analyzing the phenomena in simplified manner.

1.2. Objectives of Research

The objectives of this dissertation are to investigate two major limitations of virus filtration, protein fouling and virus breakthrough phenomena, in comprehensive and practical manners.

First, the structural and surface properties of commercial small-virus retentive filters were evaluated to reveal important affecting factors of protein fouling and virus breakthrough behaviors. Seven different commercially available membranes were used for comprehensive analysis. Membrane structures were investigated via surface and cross-section scanning electron microscopy (SEM) images. Gas-liquid porometry (GLP) analysis was performed to compare membrane pore size distributions (PSD). X-ray photoelectron spectroscopy (XPS) and surface contact angle via sessile drop methods were evaluated for membrane surface properties. In this part of dissertation, membrane performance was compared and the relationship between membrane properties and performances were defined. The first part of dissertation defined important structural parameters of virus filtration membranes for low fouling effects.

Second, virus breakthrough behavior of highly asymmetric membrane was further investigated under intensified and continuous processes. The high virus titer with intensified feed solution composition caused worsening virus breakthrough, revealed virus retention capacity of 10^{12} PFU/m^2 for commercial virus filtration membrane under conventional virus filtration process. Under the continuous virus filtration process condition with low-filtrate flux condition, severe virus breakthrough was observed virus retention less than 10^{11} PFU/m^2, due to the increased virus diffusion via low filtrate flux. The second part of dissertation

suggested optimal virus retention capacity of 10^{10} PFU/m^2 for safe filtration process, under both batch and continuous processes.

Up to date, virus filtration in biopharmaceutical downstream process research has limited by simplified manner, such as single layer filtration results or short-term filtration. The main results of this dissertation give practical insights of virus filtration process in biopharmaceutical manufacturing, for both membrane users in downstream process and next-generation virus filtration membrane development.

2. Literature Review

2.1. Virus clearance methods

For past 30 years, total 26 events of viral contamination from mammalian-cell based biopharmaceutical manufacturing have reported (Barone et al., 2020). Although the incident of viral contaminated biopharmaceutical products injection to human had not occurred, the potential risk of viral contamination of biopharmaceutical could be crucial. The source of viral contamination was from raw material to downstream process, indicated that viral contamination could occur any stage during the manufacturing process (Ajayi, Johnson, Faison, Azer, Cullinan, et al., 2022). To ensure viral safety of bio-related products, current regulation requires to apply two or more orthogonal processes for viral clearance. The clearance level has not regulated, single clearance process guarantees over 99.99% of the virus removal performance from the contaminated source (van Reis & Zydney, 2007).

Several viral clearance methods are introduced in downstream biopharmaceutical process: low pH virus inactivation, solvent/detergent virus inactivation, virus removal via chromatography, and virus retentive filtration processes (Shukla & Aranha, 2015). Low pH treatment is effective to enveloped viruses, uses pH between 3.0 to 4.0, achieved by addition of HCl or high concentrations of citric acid. Under low pH condition, however, can result the undesired aggregation of monoclonal antibodies (Wälchli et al., 2020). Solvent and detergent inactivation method is applied for products that cannot tolerate low pH treatment (Horowitz et al., 1998). Mixture of both solvent (tri-n-butyl phosphate) with detergent (Triton X100 or Tween80) are commonly used, but the low

inactivation efficient was shown under low temperature and short time treatment (Miesegaes, 2014). Virus particles can be removed during chromatographic steps, such as Protein A chromatography and anion-exchange chromatography steps. The chromatographic steps showed robust removal of retroviruses over log-reduction value (LRV) over 4, but highly depend on operational condition such as virus loading, ionic strength, and the size of columns (Miesegaes et al., 2010). Virus filtration via polymer membranes is size-based virus removal process (Johnson et al., 2022). The size-exclusion removal mechanism of virus retentive filter enabled remove both enveloped and non-enveloped viruses, without solution pH or addition of detergent. Especially, the worst-case scenario virus from Chinese hamster ovary cell-line (CHO), murine minute virus (MMV), can be effectively removed by virus filtration (Gefroh et al., 2014). The regulations did not establish minimum requirement of viral clearance capabilities, but it is known that single viral clearance process is capable of obtain LRV of 4. In downstream biopharmaceutical process, combination of low pH inactivation and virus filtration processes are widely adopted (Zydney, 2015).

2.2. Virus filtration process and membrane

2.2.1. Operating conditions

Figure 2-1 shows flow diagram of conventional biopharmaceutical production. Current regulation of mammalian-cell based biopharmaceutical requires viral safety confirmation in three major parts: virus infection check of raw materials and cell banks, validation of virus clearance capability during downstream process, and viral safety confirmation of final products (ICH, 2022). Virus filtration is mostly operated in downstream process. However, the viral contamination sources can be occurred in upstream process, virus filtration performance during upstream process is examined (Wieser et al., 2023). Virus filtration process can be applied between any stages of downstream process, but mostly applied after chromatography step and before ultrafiltration/diafiltration (UF/DF) step to minimize impact of solution impurities and concentrate on virus filtration performance (Kern & Krishonan, 2006).

Originally, virus filtration process was operated as tangential-flow filtration (TFF), the direction of applied pressure is perpendicular to flow permeate, to minimize product loss during filtration; however, current virus filtration was operated as normal-flow filtration (NFF) process, where the direction of applied pressure and flow are the same, for process simplicity and cost effectiveness (Goodrich et al., 2020). Depend on the membrane type, suggested operating pressure is varied from 98 to 298 kPa. The optimized volumetric throughput can be determined by maximum volumetric throughput analysis, plotting inverse of filtrate flux as function of filtration time, which can be expressed following equation (Peles, Fallahianbijan, et al., 2022):

$$\frac{t}{V/A} = \frac{t}{V_{max}/A} + \frac{1}{Q_0/A} \quad (2\text{-}1)$$

where t is filtration time (h) V/A is volumetric throughput (L/m^2), Q_0 is volumetric flow rate (m^3/h). The optimized volumetric throughput is determined as approximately 68% of the maximum volumetric throughput, where the filtrate flux decline of 90% occurred. However, the V_{max} analysis is solely based on pore constriction mechanism during virus filtration, the accuracy of V_{max} could be overestimated if the complicated membrane contamination mechanisms are involved, such as combined-fouling models (Ho & Zydney, 2000).

$$V_{90} = 0.68V_{max} \quad (2\text{-}2)$$

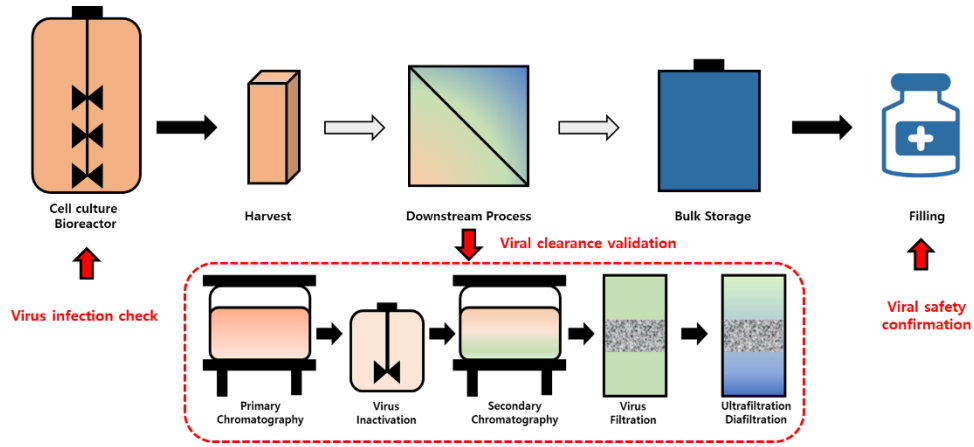

Figure 2-1. Flow diagram of commercial biopharmaceutical manufacturing process.

2.2.2. Virus filtration membrane properties

Properties of commercially available virus retentive membranes are summarized in **Table 2-1**. Current major distributors of virus filtration membrane are USA, Germany, and Japan. Commercial virus retentive membranes are polymer-based, single or multiple layers, and having different symmetricities. Virus retentive membranes were classified as large-virus removal membranes (nominal pore size of 50 nm) and small-virus removal membranes (nominal pore size of 20 nm). Currently, most of virus filtration process is adapted small-virus removal membranes due to high removal efficiency of both small and large viruses by small-virus removal membranes (Marques et al., 2009). Symmetric membranes showed nominal pore size distribution through entire membrane thickness, while asymmetric membranes had nominal pore size distribution region near lower region of the membrane.

Virus retentive membranes are mostly composed of polymers. Representative polymers used for virus filtration are hydrophilic modified polyvinylidene fluoride (PVDF), polyethersulfone (PES), and regenerated cellulose (RC), which have the advantages of low protein adsorption, high solvent resistance, broad pH durability, and high flow rate (Charcosset, 2012). To achieve low protein binding capacity, certain polymers are further hydrophilized (Johnson et al., 2022). The properties of representative polymers and properties are summarized in **Table 2-2**.

Table 2-1. Properties of commercially available virus filtration membranes (Suh et al., 2022).

Manufacturer	Model	Material	Nominal pore size	Layer	Symmetricity	Filter shape	Operating pressure	LRV from Manufacturer
Pall	Pegasus™ SV4	PVDF	20 nm	2	Symmetric	Flat sheet	2.1 – 3.1 bar	>5.5 for parvovirus
	Pegasus™ Prime	PES	20 nm	1	Asymmetric		2.1 bar	>4 for parvovirus
	Ultipor® DV50	PVDF	50 nm	3	Symmetric		1 – 2 bar	>6 for retrovirus
	Ultipor® DV20		20 nm	2			1 – 3.1 bar	>3 for parvovirus
Asahi Kasei	Planova™ BioEX	PVDF	20 nm	1	Asymmetric	Hollow fiber	2.94 bar	>5.3 for parvovirus
	Planova™ 15N	CRC	15 nm	1			0.98 bar	>4.6 for parvovirus
	Planova™ 20N		19 nm	1			0.98 bar	>5.2 for parvovirus
	Planova™ 35N		35 nm	1			0.98 bar	>5.3 for retrovirus
Millipore	Viresolve® NFP	PVDF	20 nm	3	Asymmetric	Flat sheet	2.1 bar	>6.2 for parvovirus
	Viresolve® NFR	PES	78 nm	3			2.1 bar	>6.5 for retrovirus
	Viresolve® PRO		20 nm	2			2.1 bar	>6 for parvovirus
Sartorius	Virosart® CPV	PES	20 nm	2	Asymmetric	Flat sheet	2 bar	≥4 for parvovirus
	Virosart® HC	PES	20 nm	2				≥6 for retrovirus
	Virosart® HF	PES	20 nm	1		Hollow fiber	2 bar	

Table 2-2. Overview on polymers for the membrane production (Charcosset, 2012).

Membrane material	Advantage	Disadvantage
Regenerated cellulose	- Very low unspecific adsorption - Good solvent resistance - High flow rates and high durability	- Limited stability in oxidizing agents
Modified regenerated cellulose	- Very low unspecific adsorption - Moderate flow rates. - Broad pH durability	- Ultrafilters are not to be autoclaved in dry state
Polyether sulfone	- High flow rate and high durability - Broad pH durability - High asymmetrical membrane structure available - Autoclavable in dry stae with special chemical surface modified versions	- Low to moderate unspecific adsorption (depending on surface modification) - Limited solvent resistance
Polyvinylidene fluoride	- Low unspecific adsorption - To be autoclaved in dry state - Good solvent resistance	- Moderate flow rates and durability - Hydrophobic base material; hydrophilized by surface treatment

Figure 2-2 shows SEM images of commercially available small-virus retentive membranes. Most of virus retentive membranes have non-uniform, interconnected, and having symmetric or asymmetric structures (Leisi et al., 2021; Namila et al., 2019). To minimize effect of undesired particulate and protein aggregates blocking solution transports, virus filtration is placed as skin-layer down operation; therefore, most of top structures are porous and having relatively larger pores, then the bottom structures are dense and having small pores where small viruses are captured (Syedain et al., 2006).

Figure 2-2 (a) shows the SEM image of hollow fiber membrane Planova™ 20N membrane. The image clearly indicated asymmetric structure of the membrane with different pore density through the region. **Figure 2-2 (b) and (c)** are SEM images highly asymmetric Viresolve® NFP and Viresolve® Pro membranes, where porous regions located near feed side and dense bottom regions located on bottom of the membranes. **Figure 2-2 (d)** is relatively symmetric Ultipor® DV20 membrane, clearly showed the fair pore size distributed through the membrane. Although the membranes showed different structural properties, all membranes guaranteed high virus removal performance of LRV>4.

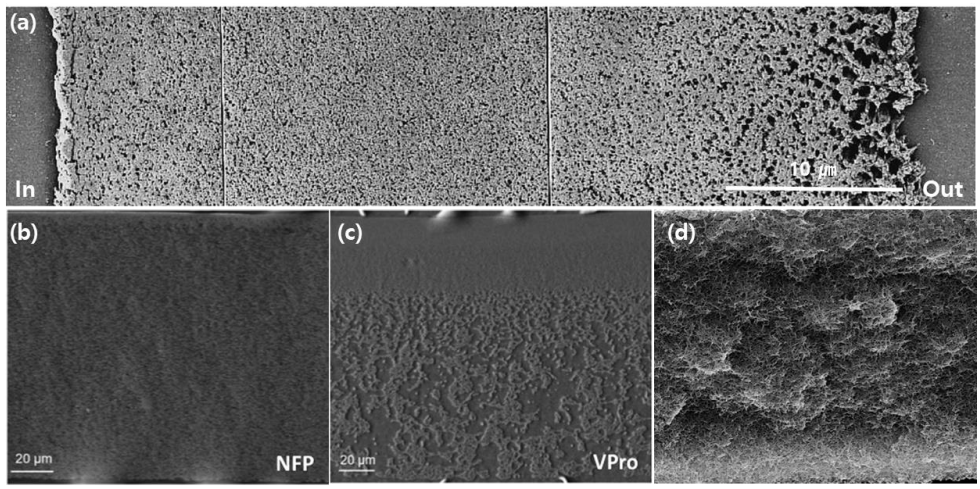

Figure 2-2. Scanning electron microscopy (SEM) Images of commercially available small virus filtration membranes (a) Planova™ 20N from Asahi Kasei (b) Viresolve® NFP from Millipore Sigma (c) Viresolve® Pro from Millipore Sigma and (d) Ultipor® DV20 from Pall (Bakhshayeshi, Jackson, et al., 2011; Fallahianbijan et al., 2019; Hongo-Hirasaki et al., 2006).

2.2.3. Membrane pore size characterization

The narrow PSD of virus filtration is important for maintaining high virus removal along with high transmission of the product. Therefore, the various PSD measurement methods were conducted, including high resolution imaging, dextran sieving test, liquid-liquid porometry, gold nanoparticle retention tests.

Dextran sieving is commonly used method for estimating PSD of MF-UF grade membranes (Bakhshayeshi, Kanani, et al., 2011). By using different sizes of dextran (500 kDa and 2,000 kDa), different pore size distribution and porosity were revealed for both asymmetric and symmetric virus filtration membranes, although the limitation of concentration polarization effect of dextran near membrane surface was shown.

Liquid-liquid porometry method is applied by using two immiscible fluids (Giglia et al., 2015). The study measured PSD of two commercially available virus filtration membranes with different hydrophilicities and structural properties, showed different PSD detection. Both membranes showed narrow PSD from 5 – 30 nm, the unexpected pore diameter from 30 – 50 nm expected to have low LRV. The measured single-layer LRV and expected LRV based on PSD measurement showed linear correlation.

Gold nanoparticle (GNP) suspension in organic solvent was effectively measured PSD of various virus filtration membrane (Kosiol et al., 2017). The organic solvent was used to prevent the undesired particle removal by adsorption of gold nanoparticles on membrane surface. The result obtained 99% cut-off pore diameter of different commercial membranes, with smaller difference between average pore diameter and 99% cut-off pore diameter was expected to achieve higher virus removal performance.

Imaging of membrane surface and cross-sections, such as SEM and transmission electron microscope (TEM) were widely used to investigate structural properties of membrane (Nazem-Bokaee et al., 2019). Recent study successfully adopted focused-ion beam SEM (FIB-SEM) technique for revealing 3D tomography of asymmetric virus filtration membrane (Brickey et al., 2021). The high-quality imaging techniques enabled to reveal not only the pore size distribution, but also pore interconnectivity and void fraction in asymmetric membrane. The effect of PSD on virus filtration performance will be discussed subsequently.

2.3. Affecting Factors of Virus Filtration Performance

2.3.1. Membrane properties

The main removal mechanism of virus filtration is size-exclusion mechanism, the virus particles retained by sieving effect (Johnson et al., 2022). Therefore, membrane structural properties were considered as the most important properties to determine overall filtration performance. The affecting structural parameters are PSD, membrane symmetricity, pore size gradients (PSGs), and pore interconnectivity. All these parameters not only affected virus removal performance, but also influence on the protein transmission.

Figure 2-3 shows the effect of average pore diameter size on model virus surrogate PP7 removal performance (Kosiol et al., 2017). The different of average 99% cut-off pore diameter is only few nanometers, but the great difference of LRVs were obtained by single layer filtration. To achieve high virus removal performance, most of membranes operated as double or triple layers, where the edge of each layer was sealed. **Figure 2-4** represents the different sizes of fluorescently labeled nanoparticles suspension on various virus filtration membranes (Fallahianbijan et al., 2017). The particle retention behaviors of were differed by membrane symmetricity. The relatively symmetric Ultipor® DV20 had 20, 40, and 100 nm nanoparticle suspension in relatively upper side of the membrane, without distinct regions for each particle size. Conversely, asymmetric Viresolve® Pro membrane, had distinguishable regions for 40 and 100 nm particles retention, with broad distribution of 20 nm particle through entire region. The different retention region of virus filtration membrane indicated the nominal pore size distribution difference, could affect on the virus removal performance. Recent

study compared the membrane PSDs by sectioning membrane single layer into 50 layers (Shirataki & Wickramasinghe, 2023). The PSD results categorized virus filtration membranes as porous asymmetric membrane, dense symmetric membrane, and laminated structure membrane. The highest virus removal performance of laminated structure membrane was obtained by more virus retention capacity, while the most stable membrane performance was observed in porous asymmetric membrane by higher porosity in virus retention region.

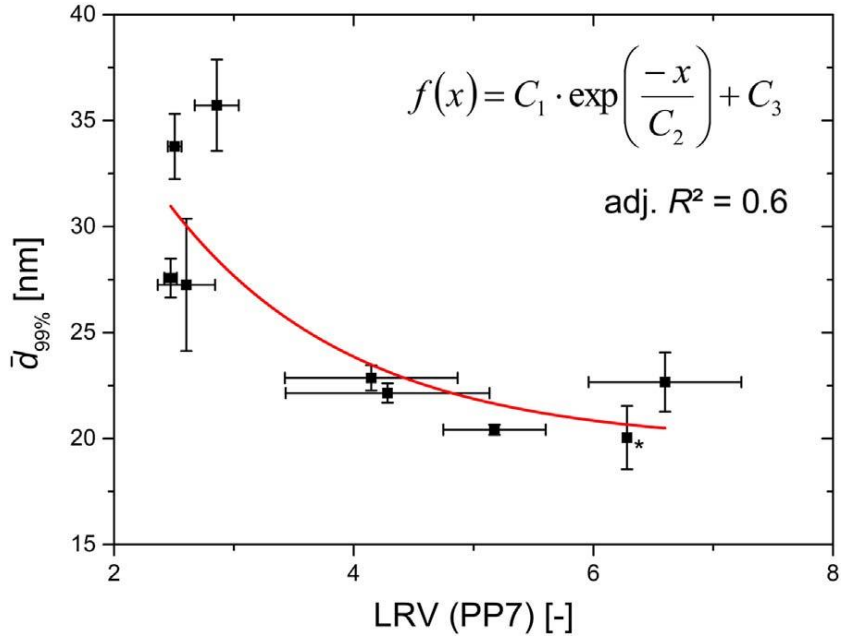

Figure 2-3. Correlation of 99% cut-off pore diameters determined from gold nanoparticle (GNP) experiments with LRVs determined using bacteriophage PP7 as accepted model virus for the set of membranes tested. The asterisk denotes filtration runs without any phages detected in the permeates (Kosiol et al., 2017).

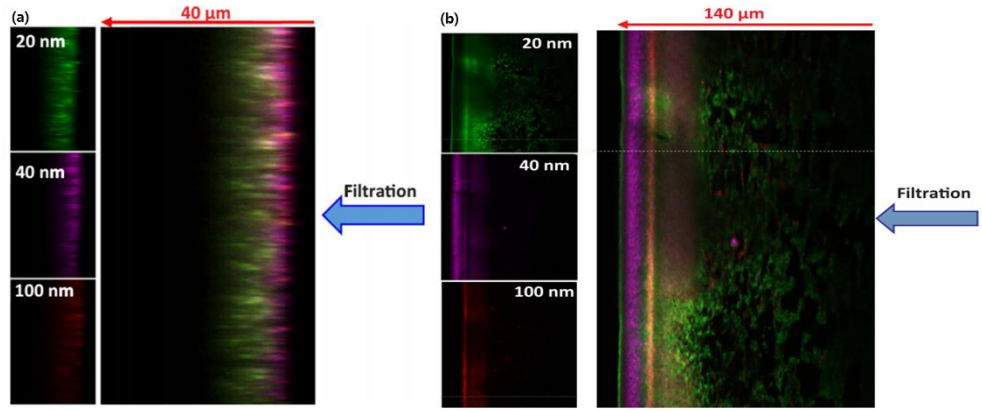

Figure 2-4. Fluorescently labeled nanoparticles retention of (a) Ultipor® DV20 membrane and (b) Viresolve® Pro membrane (Fallahianbijan et al., 2017).

Not only the PSD, but PSGs affect on the filtration performance. **Figure 2-5** shows the nanoparticle retention change by presence of protein of Viresolve® Pro membrane (Fallahianbijan et al., 2019). The Viresolve® Pro membrane, the nanoparticle retention was moved upper regions as protein fouling increased, caused stable virus retention in presence of protein. **Figure 2-6** shows the same nanoparticle retention change of Viresolve® NFP membrane. Unlike Viresolve® Pro membrane, Viresolve® NFP membrane showed no significant retention change via protein interruption. As protein deposition on membrane increased, no retention change cause undesired virus breakthrough via protein occupation in virus retention site. The different retention behaviors of Viresolve® Pro and Viesolve® NFP were caused by different PSGs near filtrate side. Viresolve® Pro showed slight pore size increase near filtrate side; however, rapid pore size increase showed in Viresolve® NFP membrane. The rapid pore size increase near filtrate side caused unexpected large molecule entrance in virus retention site, resulted more severe protein fouling and undesired virus breakthrough (Fallahianbijan et al., 2019; Kosiol et al., 2018).

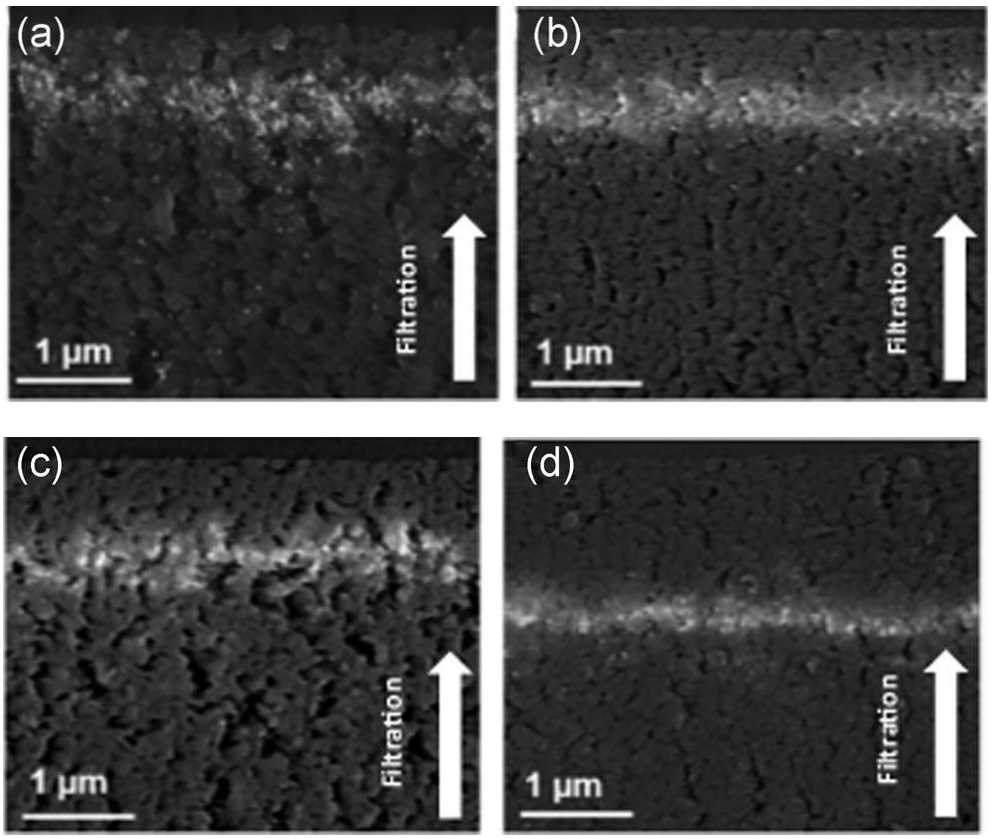

Figure 2-5. Gold nanoparticle (20 nm) retention change by protein presence in membrane. Viresolve® Pro membrane was used as model membrane. (a) clean membrane, (b) 30% flux declined membrane, (c) 60% flux declined membrane, and (d) 90% flux declined membrane (Fallahianbijan et al., 2019).

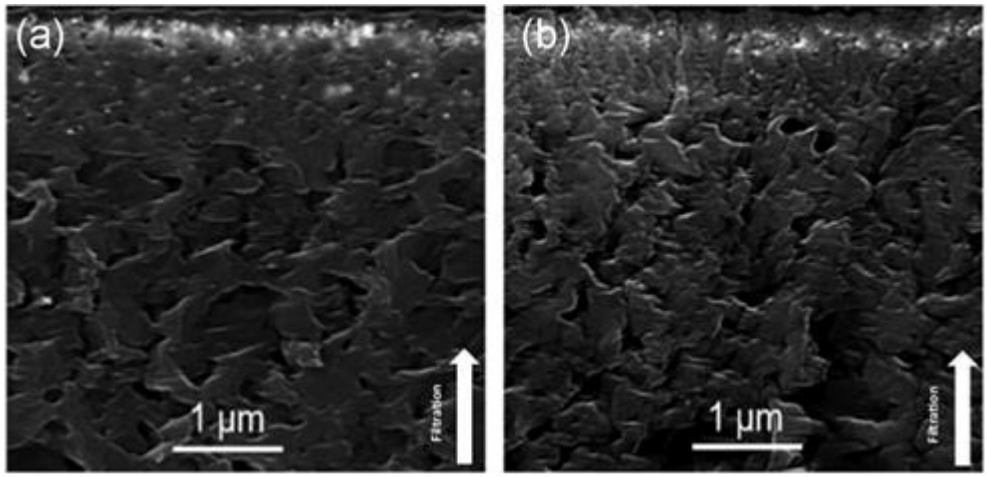

Figure 2-6. Gold nanoparticle (20 nm) retention change by protein presence in membrane with Viresolve® NFP membrane. (a) clean membrane and (b) 90% rflux declined membrane by human IgG (Fallahianbijan et al., 2019).

Most of virus filtration membranes have interconnected structure, where voids (pores) are connected to each other. The effect of pore interconnectivity on virus removal performance had been considered as negative impact, since the captured virus could be mobilized through interconnected region, caused undesired virus breakthrough (Yamamoto et al., 2014). However, recent study successfully confirmed the effect of pore interconnectivity on virus distribution in membrane (Fallahianbijan et al., 2020). The study completely blocked the certain flow path of membranes with different pore interconnectivities and compared virus retention behavior. The membranes with low connectivity showed virus retention in only open flow region, while highly interconnected membrane successfully retained nanoparticles in relatively entire region of the membrane, confirmed the interconnectivity enabled the further mitigation of nanoparticles in blocked region.

Effect of membrane material was investigated, where CRC membrane showed higher filtration capacity than PES and PVDF membranes, but the main mechanism of different filtration capacity was not clearly explained (Lute et al., 2007). Depend on the base polymer material, the membrane structures can be varied. Therefore, effect of membrane materials on virus removal performance can be limited.

Based on previous research, the virus filtration membranes are required to have narrow PSD, low increase of PSGs from membrane exit, and high interconnectivities between voids for high virus removal. However, these properties could adversely effect on other membrane performances, such as protein transmission or membrane permeability.

2.3.2. Chemical interactions

Due to the size exclusion mechanism of virus removal, the effect of chemical interactions, such as electrostatic interaction, van der Waals force and hydrophobic interaction, were considered as non-effective parameters of virus filtration performance. However, several studies investigated the effect of chemical interactions between membrane and virus. In nature, virus suspension in solution is considered as monomeric particle suspension (Gerba, 1984). The particle charge of virus in solution is determined by the isoelectric point (pI) of the virus, where the solution pH is lower than pI value, the particle charge is positively charged; conversely, the solution pH is higher than pI value, the particle is negatively charged. Most of polymers used in virus filtration membrane is negatively charged under neutral pH. **Table 2-3** summarized the commonly used model viruses in virus filtration study, with their sizes and pI values.

Table 2-3. Viruses typically used in validation studies (Heffron & Mayer, 2021; ICH, 2022; Michen & Graule, 2010).

Virus	Type	Size (nm)	Envelope	Genome	pI
MulV	Mammalian	80 – 110	Yes	RNA	4.9 – 5.0
Reovirus 3	Mammalian	60 – 80	No	RNA	3.9
SV40	Mammalian	40 – 50	No	DNA	4.7
MMV	Mammalian	18 – 26	No	DNA	4.5 – 6.2
Poliovirus	Mammalian	22 – 30	No	RNA	8.2
PPV	Bacteriophage	18 – 26	No	DNA	4.8 – 5.1
PR772	Bacteriophage	50 – 60	No	DNA	4.2 – 4.4
PhiX-174	Bacteriophage	25 – 27	No	DNA	6.0 – 7.0
PP7	Bacteriophage	25	No	RNA	4.3 – 4.9

The effect of chemical interaction between virus and membrane surface was investigated by changing solution pH or ionic strength (Dishari, Micklin, et al., 2015). Previously reported study varied solution pH and ionic strength by using bacteriophage PhiX-174, the pI of 6.6. The result demonstrated higher virus removal performance was obtained under pH 4.9 and ionic strength of 13 mM, where the bacteriophage and membrane were oppositely charged. On the other hands, the neutrally charged condition showed high virus removal performance due to possible bacteriophage aggregation neutrally charged condition, enhanced the hydrophobic interaction between bacteriophage MS2 and membrane (Van Voorthuizen et al., 2001).

Effect of chemical interaction between virus and membrane surface showed controversial results, the effect of chemical interaction was not fully understood since the chemical interaction has considered non-effective due to the size exclusion mechanism of virus filtration membranes. However, the strong effect of oppositely charged condition between virus and membrane surface result undesired virus adsorption on membrane surface, caused of increasing membrane resistance on the surface. Therefore, further investigation of various chemical interactions between membrane and virus should be fully understood.

2.3.3. Operating pressure

Conventional virus filtration process is operated as NFF for process simplicity and high product yield (Bohonak & Zydney, 2005). Depend on membrane material and module, suggested optimal applied pressure. The CRC membrane has optimal operating pressure of 98 kPa due to lower mechanical strength property of the polymer. Conversely, PVDF membrane has optimal operating pressure up to 298 kPa due to high mechanical strength (Charcosset, 2012). The optimal pressure is determined by pressure-hold test during integrity test of the membrane. Therefore, the effect of operating pressure was studied in limited aspects. However, the effect or operating pressure showed controversial result. First, the higher operating pressure caused the changing in membrane pore size, caused LRV reduction (Arkhangelsky & Gitis, 2008). Conversely, another study showed negative impact of low operating pressure, showed significant LRV reduction operating pressure under 50 kPa (Strauss et al., 2017). Currently, the downstream process is developing towards continuous process (Zydney, 2016), where no orthogonal flow is applied during downstream process. In continuous downstream process, the operating pressure (flow rate) becomes significantly lower than conventional NFF process. The effect of low operating pressure will be discussed in 2.4.

2.4. Current limitations of virus filtration process

2.4.1. Membrane fouling

Membrane fouling, the undesired membrane blocking by target removal or transport substances, inevitably occur during all membrane filtration processes. Depend on the fouling substance, the fouling can be categorized as organic fouling, inorganic fouling, colloidal fouling, and biofouling (Guo et al., 2012). Also, depend on the membrane pore size and structure, fouling mechanisms were categorized as following mechanisms: complete pore blocking, standard blocking (pore clogging), intermediate blocking, and cake filtration (Hermia, 1982). **Figure 2-7** shows the different mechanisms of membrane fouling.

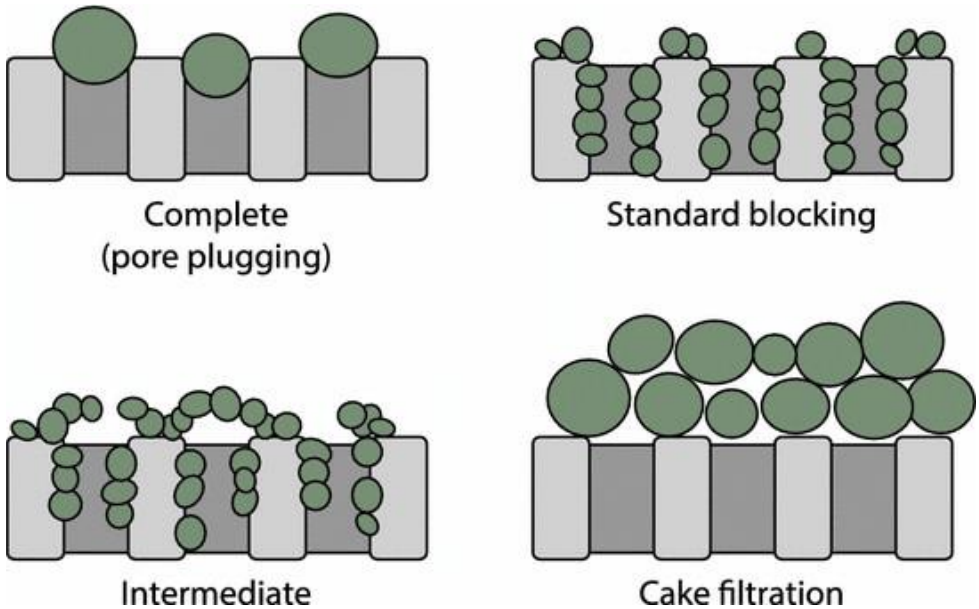

Figure 2-7. Representative membrane fouling mechanisms (Ladewig & Al-Shaeli, 2017).

Virus filtration process is also challenged by severe membrane fouling effect, showed adverse effect on filtration performances. First, the membrane fouling during virus filtration caused severe filtrate flux decline, lowering the filtration capacity. Also depend on membrane types, membrane fouling could affect virus removal performance (Bolton et al., 2005). During virus filtration, virus is captured in membrane retentive region, while proteins are effectively transmitted through the membrane. In previous studies, both virus and protein caused severe filtration capacity decrease during virus filtration (Burnouf & Radosevich, 2003). However, in real virus filtration process, virus occurrence is rare, the protein is considered as main foulant in virus filtration process. Therefore, the fouling study on virus filtration was mainly referred as protein fouling phenomenon.

Theoretically, proteins in biopharmaceuticals are smaller than the nominal pore size of virus filtration membranes, able to full transmission via size difference between membrane pore size and proteins. However, protein in nature is complicated, often existed as oligomer forms and easily form aggregates under certain condition (Wang & Roberts, 2018). The complication of protein caused severe flux decline during virus filtration. The protein fouling could be evidence of protein loss during virus filtration by undesired protein retention in virus filtration membrane, however, robust product yield was shown over >95%.

The fouling mechanism is predicted by log-log plot of the second derivative of volumetric throughput in inverse of filtrate flux and the inverse of filtrate flux, descried as following equation (Hermia, 1982).

$$\left(\frac{d^2t}{dv^2}\right) = k\left(\frac{dt}{dv}\right)^n \quad (2\text{-}3)$$

where t is filtration time, v is volumetric throughput, k is fouling constant, and n is

fouling index. The slope of log-log plot, n, determines the fouling mechanism. n value of 0, 1, 1.5, and 2 represent cake filtration, intermediate fouling, standard blocking, and complete blocking, respectively. The fouling mechanism is interchangeable during course of filtration, where the slope of log-log plot showed change as the dt/dv increase (Ho & Zydney, 2000).

Previous studies extensively revealed the effect of protein fouling in virus filtration process. First, effect of membrane orientation caused severe protein fouling propensity change, where skin-layer down operation showed higher resistance of protein fouling, due to the porous region faced feed solution acted as prefilter, reduced the degree of protein fouling near filtrate, compared to skin-layer up operation (Syedain et al., 2006).

Applying fouling models are often used to explain protein fouling mechanism during virus filtration. By assuming uniform and cylindrical pore structure, combined complete pore blockage and cake filtration model was most suitable fouling mechanism for bovine serum albumin (BSA) fouling for virus filtration membrane Viresolve® 180 (Bolton et al., 2006). The similar fouling mechanism was further confirmed by using Fc-fusion protein (size of 96 kDa) with various commercially available membranes, while different types of buffers affected on fouling propensity (Namila et al., 2019). Recent study demonstrated combined complete pore blockage and cake filtration fouling behavior of human immunoglobulin G (IgG), where the fouling parameters of complete pore blockage and cake filtration were correlated with the operating pressure (Peles, Cacace, et al., 2022).

The protein fouling can be mitigated by applying adsorptive prefilter with nominal pore size of 0.1 – 0.2 μm (Johnson et al., 2022). The adsorptive

mechanism of prefilter effectively remove large aggregates and enabled increasing virus filtration capacity. Recent study confirmed successful removal of monoclonal antibodies (mAb) aggregate of nylon prefilter due to the increase of hydrophobic interaction between protein aggregates and the membrane (Stanevich et al., 2021).

Although the fouling mechanism during virus filtration is well understood by previous studies, the negative impact of protein fouling on virus filtration is still considered as the most severe issue during virus filtration. Also, most of previous studies used single-layer operation as simplified aspects of fouling. Therefore, the protein fouling phenomena in virus filtration should focus on the similar operational conditions as real virus filtration process.

2.4.2. Virus breakthrough

Although virus filtration process provides robust virus removal performance, undesired virus breakthrough could occur. The observed virus breakthrough conditions under virus overloading during long-term operation (Lute et al., 2007), sever flux decline (Bolton et al., 2005), sudden flow interruption during or after filtration (Dishari, Venkiteshwaran, et al., 2015; LaCasse et al., 2016; Leisi et al., 2021), and low flow rate operation (Fan et al., 2021; Yamamoto et al., 2014). The breakthrough propensity can be differed by type of membrane and structural differences (Afzal & Zydney, 2022).

The virus retention capacity of virus filtration membranes is finite, and each membrane has different virus retention capacity. Once the retention capacity of virus filtration membrane is occupied, the virus particles could be redirected to relatively larger pores, caused severe virus breakthrough. Previous study compared virus removal performance of early developed small virus filtration membranes and revealed the virus loading over 10^{14} PFU/m^2 caused phage-dominant process disruption, rather than protein fouling (Lute et al., 2007). The virus removal behavior was differed by membranes, although the study clearly indicated that the robust virus removal performances of all tested membranes. The mechanism of virus breakthrough was further investigated by using mechanistic modeling (Rathore et al., 2014), considered the ratio between nominal pore size of each membrane and the particle diameter of model virus surrogate. The mechanistic model successfully correlated the experimental data, enabled to predict virus removal performance decline under virus overloading.

Severe flux decline by protein fouling was considered as main reason for virus breakthrough, by pre-occupation of virus retention site by protein fouling (Bolton

et al., 2005). The flux decline during virus filtration was presumed that the virus is flow through relatively larger pores of the membrane. The flux decline related virus removal performance for multi-layers virus filtration membrane can be predicted as following equation:

$$LRV = -\log\left(\frac{S_l \delta Q_0}{Q}\right)^n = LRV_0 - nlog\left(\frac{Q_0}{Q}\right) \quad (2\text{-}4)$$

where S_l is sieving coefficient of the combined flow through the large pores, δ is the fraction of initial flow rate through large pores, n is the number of layers, Q_0 is the total initial flow rate, and Q is the flow rate. The study correlated the flux decline during filtration is related to the LRV reduction, rather than the LRV reduction as function of volumetric throughput increase by using Viresolve® NFP membrane.

Regarding effect of protein fouling on virus breakthrough, however, converse result was obtained by using relatively symmetric virus filtration membrane Ultipor® DV20 (Jackson et al., 2014). The membrane proposed the LRV reduction mechanism as internal concentration polarization effect, where virus accumulation near membrane surface, caused concentrated virus near membrane challenged during virus filtration process, while the impact of protein fouling was minimal. The internal concentration polarization model was described as following equation:

$$LRV = -[nlog(xS) + \log(n!)] - nlog\left(\frac{V}{V_R}\right) \quad (2\text{-}5)$$

where n is number of layers, S is virus sieving coefficient of membrane, V is filtrate volume, and V_R is volume of reservoir zone, the volume of virus accumulated near membrane surface. The V_R was estimated by visualization of model virus surrogate deposition on the membrane by confocal laser scanning microscopy (CLSM). The model successfully predicted virus removal performance

of both clean membrane and pre-fouled membrane up to 50% of initial flux decline.

During virus filtration, unexpected flow interruptions were occurred in multiple scenarios such as using multiple reactor chamber for single virus filtration, in prior to buffer flush for product recovery, and sudden shut down of filtration process (LaCasse et al., 2016). The unexpected virus breakthrough was observed after re-pressurization after flow interruption (Asper, 2011). **Figure 2-8** shows the phage migration before and after flow interruption, by challenging differently labeled fluorescent tagged bacteriophage. The visualization of model virus surrogate confirmed that virus migration occurred before/after flow interruption (Woods & Zydney, 2014). The main reason of virus migration during flow interruption can be explained by increase of the Brownian motion of the virus. The increase of Brownian motion was considered as problematic of virus retention behavior, since the virus retention site larger than virus could not constrict virus solely, exposure to potential risk of virus mitigation through interconnected structure (Yamamoto et al., 2014). The virus breakthrough increased under the longer period of flow interruption, supported the Brownian motion dependent virus breakthrough behavior (LaCasse et al., 2016). Under low pressure condition where the Peclet number becomes less than 1, the virus diffusion dominant flow condition could be resulted undesired virus breakthrough. The study revealed the effective diffusivity of virus in membrane becomes two orders of magnitude lower than diffusivity under free condition. In case of the virus size of 20 – 21 nm diameter, the critical flux that becomes diffusive flow dominant condition was assumed to be ~17 LMH (Fan et al., 2021). Once the flux is lower than the critical flux, severe flux decline was observed under low flux condition.

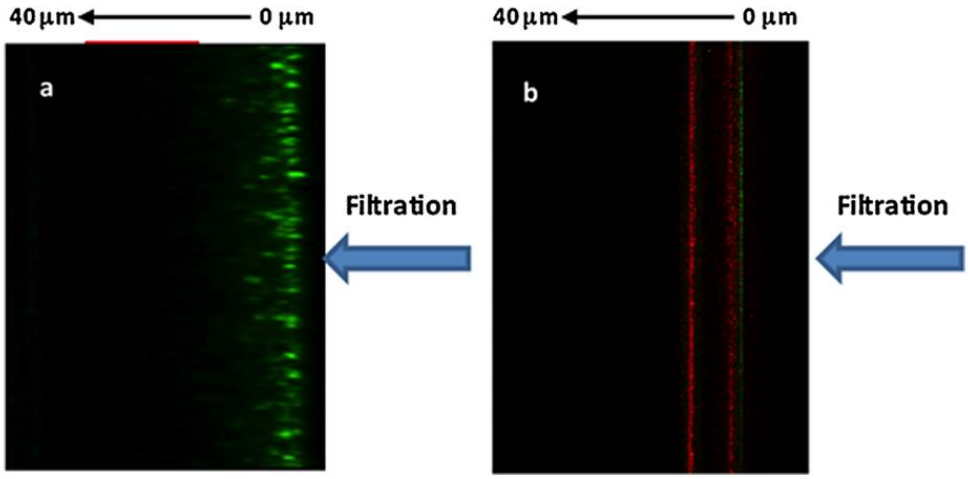

Figure 2-8. Cross-sectional images of Ultipor® DV20 membranes after filtration of fluorescently labeled PhiX-174 at constant pressure (left) and after a flow interruption experiments (right). The Cy5-labeled (red) phage was used in the challenge before the pressure release, with the SYBR gold labeled (green) phage used after pressure release (Dishari, Venkiteshwaran, et al., 2015).

2.4.3. Virus filtration process for continuous process

As mentioned in previously section, current downstream development is focused on ‘continuous’ downstream process, where no orthogonal process is applied during downstream process. The characteristic of continuous downstream process is operating with low flux to balance out the entire process stream. However, under low flux operation, virus breakthrough could be crucial. Previous research aimed to validate the capability of commercial virus filtration membranes for continuous process (David et al., 2019). The study obtained 72 h operation of virus filtration with flow rate of 0.3 LMH. The used virus filtration membranes were confirmed its high removal performance in conventional virus filtration process; however, the severe virus removal performance decline was observed for early-developed virus removal filtration membranes. Since current virus filtration membranes were designed for orthogonal process, adopting current virus filtration membrane to continuous process must be validated in terms of virus removal performance and flux behaviors.

Another concern of continuous downstream process is the increased concentration of protein by high product yield from cell culture and harvest process (Müller et al., 2022). The high concentration of product enabled the mass production of biopharmaceutical under the same process capacity; however, the high concentration of protein could cause severe filtrate flux decline during virus filtration, caused delay of later processes by flux decline in virus filtration step. Therefore, clear understanding of protein fouling and virus breakthrough phenomenon under continuous process clearly investigated.

3. Evaluation of virus filtration membrane properties and its relationship with filtration performances

3.1. Introduction

Viral contamination from mammalian cell-based biopharmaceutical production has threatened product safety (Ajayi, Johnson, Faison, Azer, Cullinan, et al., 2022). Viral safety during biopharmaceutical manufacturing processes must be ensured, and it has been stated to use at least two independent methods for reproducible reduction of viral load in the order of 4 logs or more (ICH, 2022). Virus filtration provides robust and effective virus removal capabilities without adversely impacting product safety (Johnson et al., 2022). Virus-retentive membranes are composed of polymers such as hydrophilic modified polyvinylidene difluoride (PVDF), polyethersulfone (PES), or cuprammonium regenerated cellulose (CRC), which are known to have robust mechanical strength, an asymmetric or a symmetric membrane structure, and a low protein binding capacity (Burnouf & Radosevich, 2003; van Reis & Zydney, 2007). The virus filtration mechanism primarily relies on size exclusion to remove the viruses, where the retentive region of the membrane with a pore size of 15 – 20 nm effectively captures viruses of similar size (e.g. murine minute virus (MMV) with a size of 18 – 26 nm) (Gefroh et al., 2014). Meanwhile, biopharmaceuticals (such as monoclonal antibodies (mAb) with a size of 9 – 12 nm) pass through the membrane without being captured (Adan-Kubo et al., 2019; Bakhshayeshi, Jackson, et al., 2011; Esfandiary et al., 2013; Yamamoto et al., 2014).

Despite the high virus removal performance (i.e., >4 $\log_{10}$) with >95% of product yield, virus filtration is still limited by protein fouling, which results in

decreased filtration capacity and virus breakthrough. Previous studies have investigated the protein fouling issue in virus filtration in terms of membrane properties, operational conditions, and feed solution conditions. For example, Syedain et al. (2006) showed that filtration with the skin-layer on the upward direction of the Viresolve®180 membrane caused more severe fouling due to rapidly increased membrane resistance via deposited bovine serum albumin (BSA). Marques et al. (2009) investigated the effects of membrane materials on protein fouling behavior and found that a CRC membrane (i.e., Planova™ 20N) showed stabilized filtrate flux with 4 – 20 g/L of human immunoglobulin G (IgG) whereas PES and PVDF membranes (i.e., Virosart® CPV and Viresolve® NFP, respectively) showed flux decay before 50 L/m^2. Lute et al. (2007) reported that high virus retention over ~10^{14} PFU/m^2 caused both flux decay and virus breakthrough as the virus occupied a finite number of retention sites. A linear relationship between log-reduction value (LRV) reduction and flux decay was demonstrated by Bolton et al. (2005) through a filtration experiment using the Viresolve® NFP membrane, φX-174 as a model virus, and BSA as a model protein.

Protein fouling behaviors between ultrafiltration membranes and Ultipor® DV20 were compared, whose results showed similar complete blocking behaviors (Wickramasinghe et al., 2010). Bolton et al. (2006) proposed a combined model of cake filtration and complete blocking which was most suitable for Viresolve® 180 membrane with BSA solution. This combined fouling behavior was also well described using disc-type PES and hollow fiber-type CRC membranes with Fc-fusion proteins (Namila et al., 2019). Recently, Peles et al. (2022) proposed a global pore blockage-cake filtration model including pressure effects on protein

fouling with human IgG using Viresolve® Pro membrane. The model indicated that as pressure increased, the intermediate pore blockage parameter decreased while the cake filtration parameter increased in the pressure range of 0.2 to 60 psi. Shirataki et al. analyzed protein fouling when using plasma IgG solution with Planova™ BioEX membranes by a simple generalized filtration equation, independent of a particular blocking model derived from the characteristic form (Shirataki et al., 2021). Previous studies have shed light on protein fouling during virus filtration, however, there is still a need to better understand it in commercially available virus-retentive membranes made of different materials, modules, and the number of layers.

This study aimed to investigate the effects of protein fouling on filtrate flux and virus breakthrough of commercial membranes under the same feed compositions (i.e., bacteriophage MS2 as a model virus and BSA as a model protein). Classical fouling models (i.e., complete blocking, standard blocking, intermediate blocking, and cake filtration models) were applied to determine the most suitable model for protein fouling during virus filtration. The nominal pore size and distribution in retentive regions of membranes were observed through scanning electron microscopy (SEM) to study their potential impact on protein fouling behaviors. Seven commercial virus membranes have different behaviors of protein fouling, presented by filtrate flux and virus breakthrough, which are well-suited for different fouling models (mostly standard blocking). These results provide important insights into the factors controlling the protein fouling phenomenon during virus filtration in the biopharmaceutical manufacturing process.

3.2. Materials and Method

3.2.1. Materials

Seven commercial membranes were used for virus filtration, obtained from Asahi Kasei Medical Co., Ltd. (Japan), Merck Millipore Ltd. (USA), Pall Corp. (USA), and Sartorius Stedim Biotech (Germany). The properties of commercial virus-retentive membranes used in this study are summarized in **Table 3-1**. The used membranes were composed of PVDF, PES, or CRC.

Escherichia coli (E. Coli) bacteriophage MS2 (ATCC-15597-B1) and *Pseudomonas aeruginosa* bacteriophage PP7 (ATCC-15692-B4) were used as small virus surrogates, purchased from the American Type Culture Collection (ATCC®, USA). The propagation procedure from the ATCC® product sheet was used for bacteriophage propagation and purification. Purified bacteriophage stocks were stored at 4°C. BSA (Millipore Sigma, USA) was used as a model protein. A protein-suspended solution was prepared by dissolving BSA powder in 10 mM of bioperformance-certified phosphate buffer saline (PBS; Millipore Sigma, USA) solution at pH 7.4, followed by vacuum filtration with a 0.2 μm hydrophilic PVDF membrane filter (Hyundai Micro, Republic of Korea) to remove undesired particulates or protein aggregates.

Table 3-1. Summary of commercial virus filtration membranes used in this study.

Manufacturer	Membrane	Material	Module	Layers	Effective area (cm^2)	Operating pressure (bar)
Asahi Kasei Medical Co., Ltd.	Planova™ BioEX	PVDF	Hollow fiber	1	3.0	3
	Planova™ 20N	CRC	Hollow fiber	1	10.0	1
Merck Millipore Ltd.	Viresolve® NFP	PVDF	Syringe	3	3.5	2
	Viresolve® Pro	PES	Syringe	2	3.4	2
Pall Corp.	Pegasus™ Prime	PES	Syringe	2	2.8	2
	Pegasus™ SV4	PVDF	Disc	2	13.8	3
Sartorius Stedim Biotech	Virosart® CPV	PES	Syringe	2	5.0	2

3.2.2. Virus filtration process

Figure 3-1 shows the scheme of virus filtration process used in this study. In this study, constant pressure virus filtration was performed with operating pressure from 1 to 3 bar. Prior to the virus filtration experiments, a pure buffer filtration was performed for 30 min to membrane wetting and to remove air trapping in the system. After pure buffer filtration, the feed solution was switched to a model feed solution to perform virus filtration experiments. Feed solution filtration was performed up to 300 L/m^2 or filtrate flux decline over 60%. The filtrate flux was calculated by measuring the weight change and was expressed as LMH. To analyze virus breakthrough and protein transmission, grab sample was collected every 50 L/m^2 during filtration experiments.

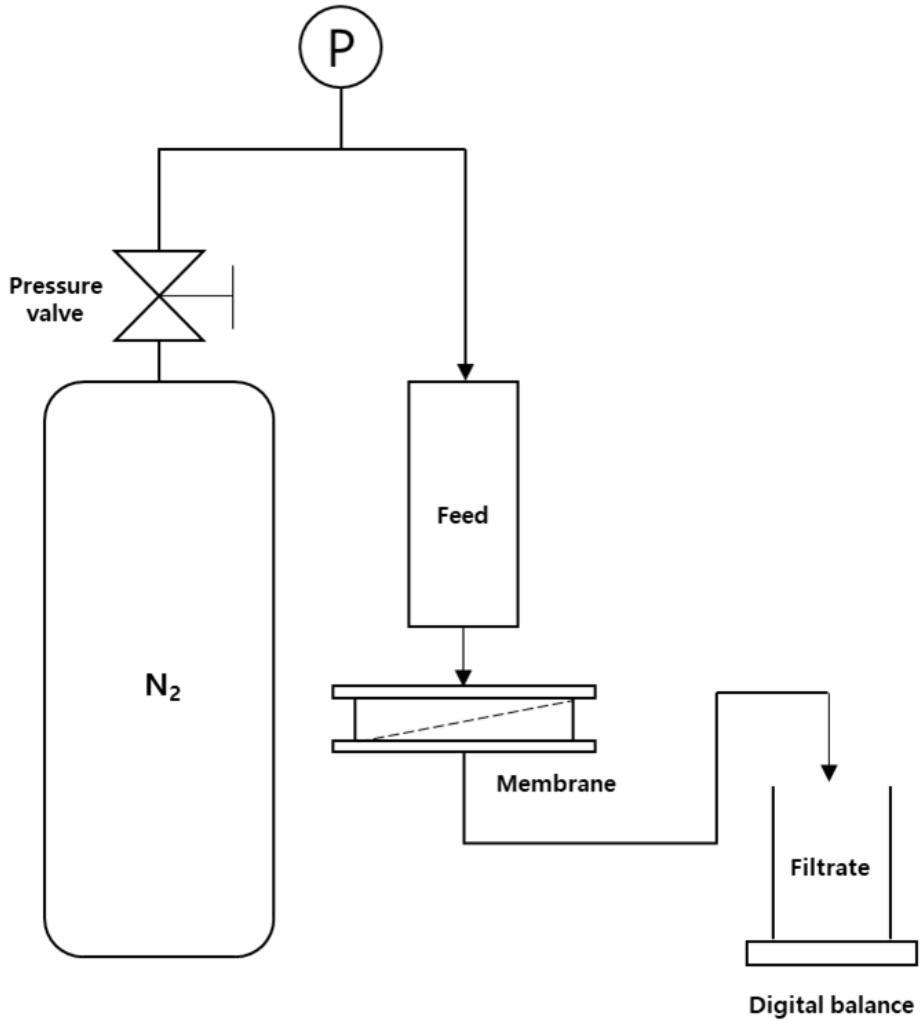

Figure 3-1. Scheme of normal-flow filtration virus filtration process.

3.2.3. Analysis

Membrane morphologies were analyzed by SEM (SigmaHD, Carl Zeiss, Germany). In the top / bottom and cross-sectional images, an applied voltage of 3.0 kV and magnification ranging from 500 to 40,000 zoom captured the best images for membrane structure observation. The membrane properties, such as pore diameter, thickness, and surface porosity, were measured using 'Image J' software.

The phage titer in the feed and filtrate solutions were quantified using the double-layer agar method for plaque-forming assay. The collected feed or filtrate samples were mixed with 24 h grown 200 μL of host cells in ATCC® medium 271 (*Escherichia* medium) containing 0.5% agar solution. The mixed solution was poured directly into the bottom agar containing 1.5% agar medium. Hardened agar plates were incubated for at least 6 – 8 h at 37°C. Bacteriophages were visible as clear dots on the agar surface. For virus titers higher than 10^3 PFU/mL, serial 10-fold dilutions were performed until the solution had no more than 10^3 PFU/mL. LRV was calculated according to following equation.

$$LRV = -\log\left(\frac{C_{filtrate}}{C_{feed}}\right) \quad (3\text{-}1)$$

where $C_{filtrate}$ and C_{feed} are the virus concentrations in filtrate and feed, respectively.

BSA and human IgG were characterized by size exclusion chromatography using a Waters Alliance 2695 HPLC (Waters corp., USA) equipped with TSKgel G3000SWXL column (Tosoh corp., Japan) and Waters 2998 PDA detector to determine their molecular weights, shown in **Figure 3-2**. Protein concentration was measured by UV-vis absorbance at a wavelength of 280 nm to determine protein

transmission.

Membrane pore size distribution was examined by GLP method. For GLP analysis, Viresolve® Pro, Viresolve® NFP, Virosart® CPV, and Pegasus™ SV4 membranes were used. The nominal pore size between GLP analysis and SEM imaging detections were compared to correlate nominal pore sizes.

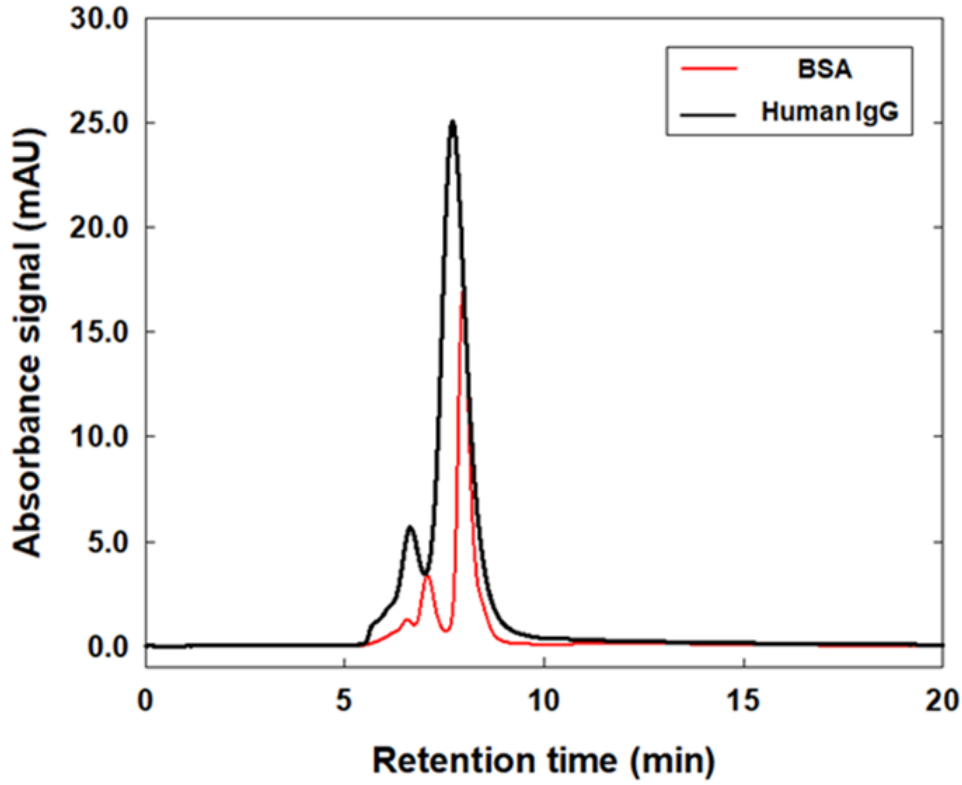

Figure 3-2. Size exclusion chromatogram for 1 g/L of BSA and human IgG in 10 mM PBS at pH 7.4

3.2.4. Confocal laser scanning microscopy (CLSM) analysis

To confirm fouling mechanism, 2 g/L of fluorescent-tagged albumin was filtered with single-layer Viresolve® Pro and Pegasus™ SV4 membranes. Filtration process is performed over 50 L/m^2 to observe filtrate flux decline by fluorescent-tagged albumin. The filtered membranes were further examined with confocal laser scanning microscopy (CLSM, LMS 510 META, Carl Zeiss, Germany) with x63 and x100 oil immersion lens.

To prepare cross-section membrane samples, fluorescent-tagged albumin filtered membranes were embedded in paraffine. The embedded membrane was cut orthogonally with thickness of 15 μm by using microtome (Leisi et al., 2021). To fluorescent observation, 488 nm wavelength was chosen.

3.3. Results and Discussion

3.3.1. Membrane characterization

Figure 3-3 shows SEM images of the top surface, cross-section, retentive region, and bottom surface of the commercial virus-retentive membranes. Membrane single layer thickness, top surface pore diameter, and nominal pore diameter in the retentive region are summarized in **Table 3-2**. SEM images of cross-section and retentive regions enabled the determination of membrane symmetricities for the following: Pegasus™ SV4, Virosart® CPV, Viresolve® NFP, Pegasus™ Prime, and Viresolve® Pro. Membrane symmetricities of hollow fiber membranes, Planova™ BioEX and Planova™ 20N, could not be clearly determined using SEM images as these membranes are known to be asymmetric, with relatively narrower PSD through entire region than other asymmetric membranes (Adan-Kubo et al., 2019; Nazem-Bokaee et al., 2019). The cross-section image of Viresolve® Pro showed three distinct regions: an upper 60 μm region of relatively porous structure with larger pores, a middle denser region of 40 μm with large pores, and a bottom 40 μm region of small pores distributed throughout. Pegasus™ Prime and Viresolve® NFP had two distinctive regions: a thicker, larger pore region and a thin virus-retentive site. The porous and retaining regions were barely distinguishable in cross-section SEM images of Virosart® CPV and Pegasus™ SV4. However, the retentive region images allowed for the comparison of the nominal pore diameter, which was close to 20 nm. Viresolve® Pro, Pegaus™ Prime, and Viresolve® NFP had the smallest pore diameters near the filter exit, a similar pore diameter near the bottom surface. Virosart® CPV had the 20 – 30 nm pore diameter region located 6 μm above the membrane exit.

Pegasus™ SV4 showed a relatively even distribution of both large (80 – 100 nm) pores and small pores (30 – 40 nm) throughout the entire region. Viresolve® Pro, Pegasus™ Prime, and Virosart® CPV showed average pore diameters from 16.4 to 28.4 nm in the retentive region. Viresolve® NFP and Pegasus™ SV4 showed nominal pore diameters of 45.9 ± 13.7 and 33.7 ± 11.1 nm, respectively. It was noted that 2D image analysis for membrane morphology had some limitations, such as limited estimation of the circular shape of pores, discrepancy of cross-sectional pore structure, and limited analysis of pore interconnectivity. Although 3D image analysis, for example using FIB-SEM tomography, provides better interpretation (Brickey et al., 2021), 2D SEM images can be used to simply distinguish structural differences among virus-retentive membranes. The difference in membrane structure and nominal pore size suggested that different fouling propensities and virus removal performances are expected under the same experimental conditions.

In addition to SEM images, gas-liquid prometry data of Viresolve® Pro, Viresolve® NFP, Virosart® CPV, and Pegasus™ SV4 membranes were obtained to compare nominal pore size and pore size distribution. As seen **Figure 3-4,** varied PSD profiles were obtained by each membrane, as seen in their SEM images. Viresolve® Pro and NFP showed narrow PSD with relatively larger average pore size of NFP; in contrast, Virosart® CPV and Pegasus™ SV4 obtained broad PSD. The measured average pore diameter of Viresolve® Pro, Viresolve® NFP, Virosart® CPV, and Pegasus™ SV4 were 21.6, 23.5, 22.6 and 23.4 nm, respectively.

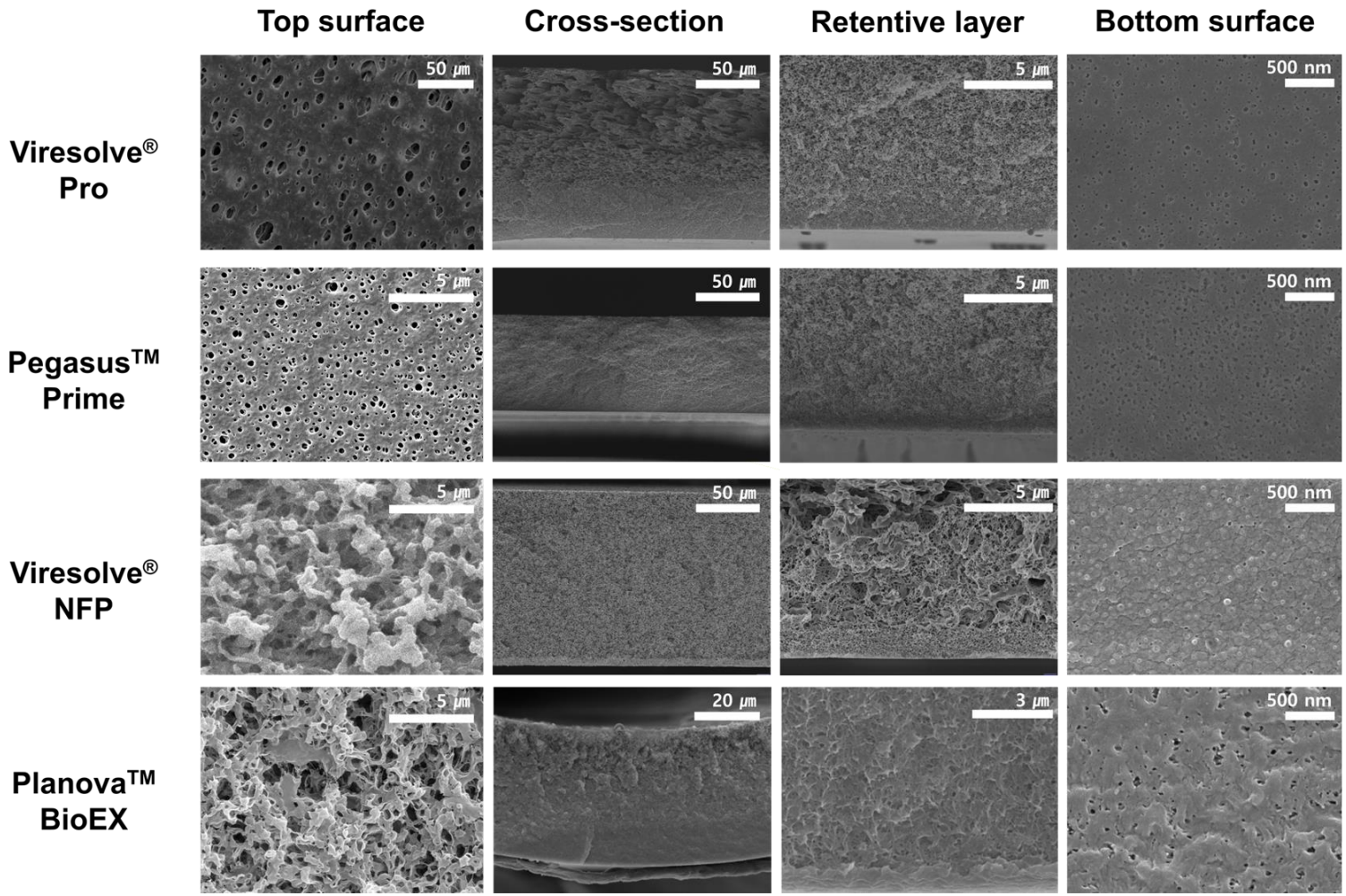
Top surface
Cross-section
Retentive layer
Bottom surface
Viresolve® Pro
Pegasus™ Prime
Viresolve® NFP
Planova™ BioEX
50 μm
50 μm
5 μm
500 nm
5 μm
50 μm
5 μm
500 nm
5 μm
50 μm
5 μm
500 nm
5 μm
20 μm
3 μm
500 nm

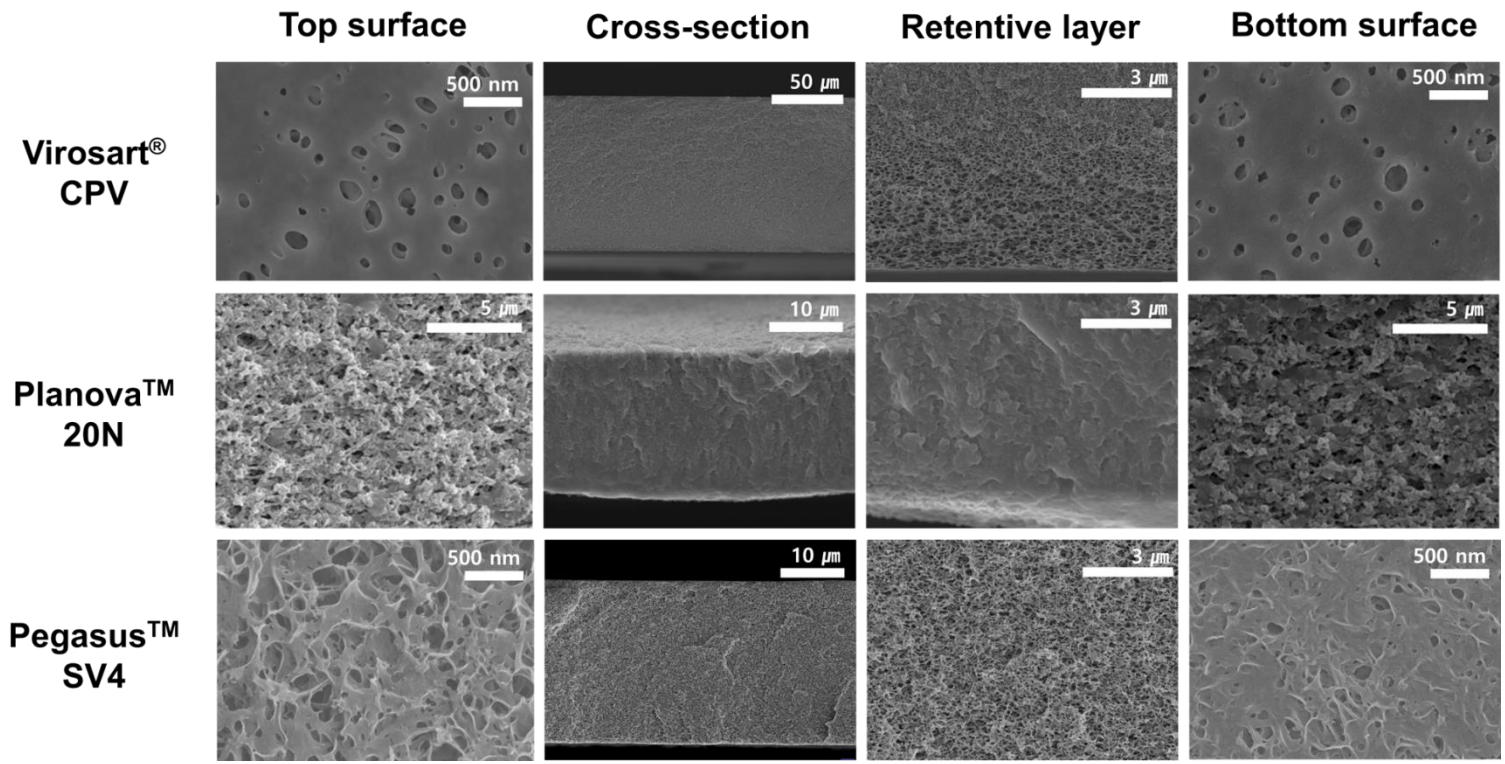

Figure 3-3. SEM images of commercial small virus-retentive membranes.

Table 3-2. Single layer thickness, top surface pore diameter, and nominal pore diameter of commercial virus filtration membranes.

	Viresolve® Pro	**Pegasus™ Prime**	**Viresolve® NFP**	**Planova™ BioEX**	**Virosart® CPV**	**Planova™ 20N**	**Pegasus™ SV4**
Single layer thickness (μm)	140	80	140	40	110	20	25
Top surface pore diameter (μm)	3.0 ± 2.0	0.2 ± 0.4	0.3 ± 0.1	0.2 ± 0.1	0.1 ± 0.04	0.2 ± 0.04	0.1 ± 0.02
Nominal pore diameter (nm)[†]	27.2 ± 6.0	16.4 ± 5.8	45.9 ± 13.7	n.a.	28.4 ± 8.3	n.a.	33.7 ± 11.1

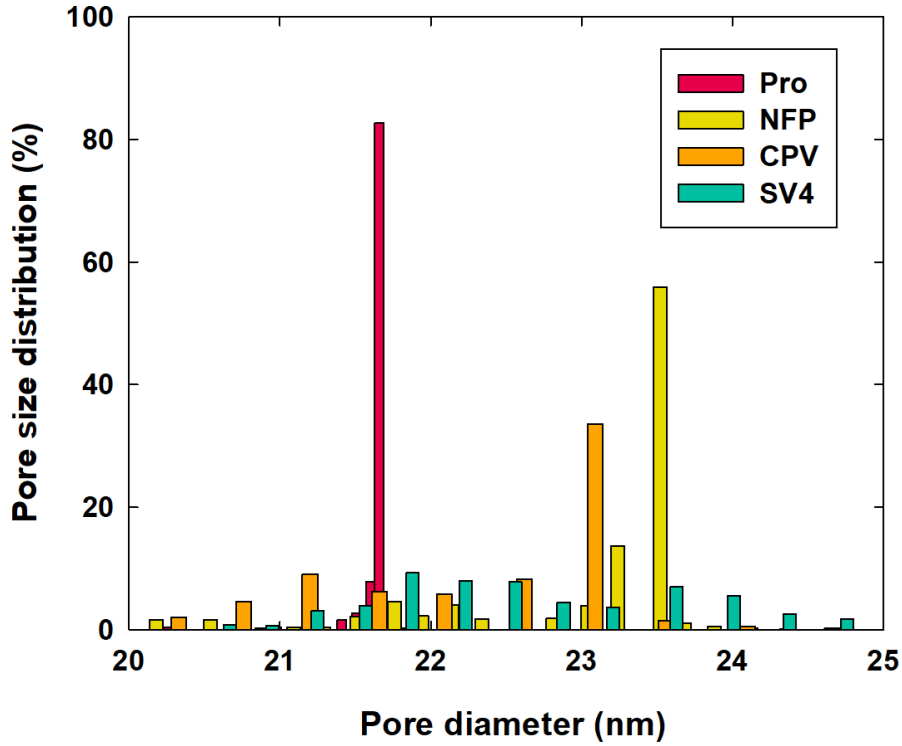

Figure 3-4. Pore size distribution (PSD) of Viresolve® Pro, Viresolve® NFP, Virosart® CPV, and Pegasus™ SV4 membranes. PSD was measured by gas-liquid porometry (GLP).

Chemical composition and hydrophobicity of membrane surfaces were analyzed using X-ray photoelectron spectroscopy and contact angle analyzer, and results are summarized in **Table 3-3**. As expected, results of chemical composition were represented each material (i.e., PVDF, PES, or CRC). Additional sulfur and nitrogen peaks observed in PES membranes and PVDF membranes showed an oxygen peak. In terms of surface hydrophobicity, Pegasus™ Prime had a hydrophilic surface (i.e., <20° of contact angle), while Viresolve® NFP had a hydrophobic surface (i.e., 114° of contact angle). Other membrane contact angles were in the range of 63 – 92° except Planova™ 20N which was immediately wet during the measurement.

Table 3-3. X-ray photoelectron spectroscopy (XPS) and contact angle data for virus-retentive membranes.

Membrane	Material	Element composition in atomic concentration (%)†					Contact angle(deg)
		Carbon	Oxygen	Sulfur	Fluorine	Nitrogen¶	
Viresolve® Pro	PES	74.2	21.0	3.6	-	0.4	70‡
Pegasus™ Prime	PES	74.8	18.3	4.0	-	2.7	<20‡
Viresolve® NFP	PVDF	56.2	2.7¶	-	41.1	-	114‡
Planova™ BioEX	PVDF	51.7	4.1¶	-	44.1	-	85§
Virosart® CPV	PES	75.5	17.7	4.0	-	2.3	63‡
Planova™ 20N	CRC	61.8	38.2	-	-	-	N/A§
Pegasus™ SV4	PVDF	55.7	3.9¶	-	40.4	-	92‡

† analyzed by Axis Nova (Shimadzu, Japan)

‡ Contact angle measured using sessile drop method (DSA300, KRÜSS, Germany)

§ Contact angle measured using Wilhelmy method (Sigma 701, KSV Instruments Ltd, USA) Noted that Planova™ 20N was rapidly wet during the measurement which showed <5°.

¶ Unexpected oxygen peaks from PVDF membranes and nitrogen peaks from PES membranes indicated further hydrophilic treatment after membrane fabrication, although the treatment method is unknown.

3.3.2. Effect of protein fouling and its affecting factors

The filtrate flux results for PBS solution and feed solution (comprised of 1 g/L BSA and ~10^7 PFU/mL MS2 bacteriophage in 10 mM PBS solution at pH 7.4) for seven commercial virus-retentive membranes are summarized in **Table 3-4**. The buffer flux of each membrane at optimal operating pressure varied from 45.7 to 511.5 LMH; the highest flux was observed in Viresolve® Pro, and the lowest flux was observed in Pegasus™ SV4. Different membrane morphologies, such as membrane thickness, PSD, porosity, and nominal pore diameter of the bottom layer, could have resulted in different filtrate flux behaviors (Wickramasinghe et al., 2010). Membranes with higher initial flux such as Viresolve® Pro, Pegasus™ Prime and Viresolve® NFP showed a large immediate flux decline while other membranes showed insignificant flux decline. This is possibly due to the effect of concentration polarization and/or protein fouling during the flux measurement (i.e. 5 min). It is noted that high BSA transmissions over 95% were seen in all membranes regardless of the flux decay.

Table 3-4. Filtrate fluxes of virus-retentive membranes with 10 mM of PBS or feed solution.

Filtrate flux (LMH)	Viresolve® Pro	Pegasus™ Prime	Viresolve® NFP	Planova™ BioEX	Virosart® CPV	Planova™ 20N	Pegasus™ SV4
PBS buffer	511.5 ± 13.7	473.0 ± 45.8	395.6 ± 40.1	150.6 ± 4.0	121.9 ± 11.4	75.4 ± 1.5	45.7 ± 1.1
Feed solution†	447.1 ± 6.6	346.7	183.7	142.4 ± 5.1	109.6 ± 4.4	68.3 ± 3.6	43.2 ± 1.3

† Feed solution was composed with 1 g/L of BSA with ~10^7 PFU/mL MS2 bacteriophage in 10 mM PBS solution at pH 7.4.

Figure 3-5 shows the filtrate flux behavior during virus filtration with the feed solution as a function of volumetric throughput of up to 80 – 300 L/m^2. Data were obtained from two to four replicates, besides Pegasus™ Prime and Viresolve® NFP. Note that some error bars are invisible due to their small values for Viresolve® Pro, Planova™ 20N, and Pegasus™ SV4. Planova™ BioEX, Planova™ 20N, and Pegasus™ SV4 showed 10 – 14% of flux decay ranging from 170 – 300 L/m^2 of volumetric throughput. Other membranes showed more severe flux decay: 60% for Viresolve® Pro until 300 L/m^2, 86% for Pegasus™ Prime until 285 L/m^2, 66% for Virosart® CPV until 150 L/m^2, and 82% for Viresolve® NFP until 80 L/m^2. The order of the fouling propensity is as follows: Planova™ 20N, Planova™ BioEX, Pegasus™ SV4, Viresolve® Pro, Pegasus™ Prime, Virosart® CPV, and Viresolve® NFP.

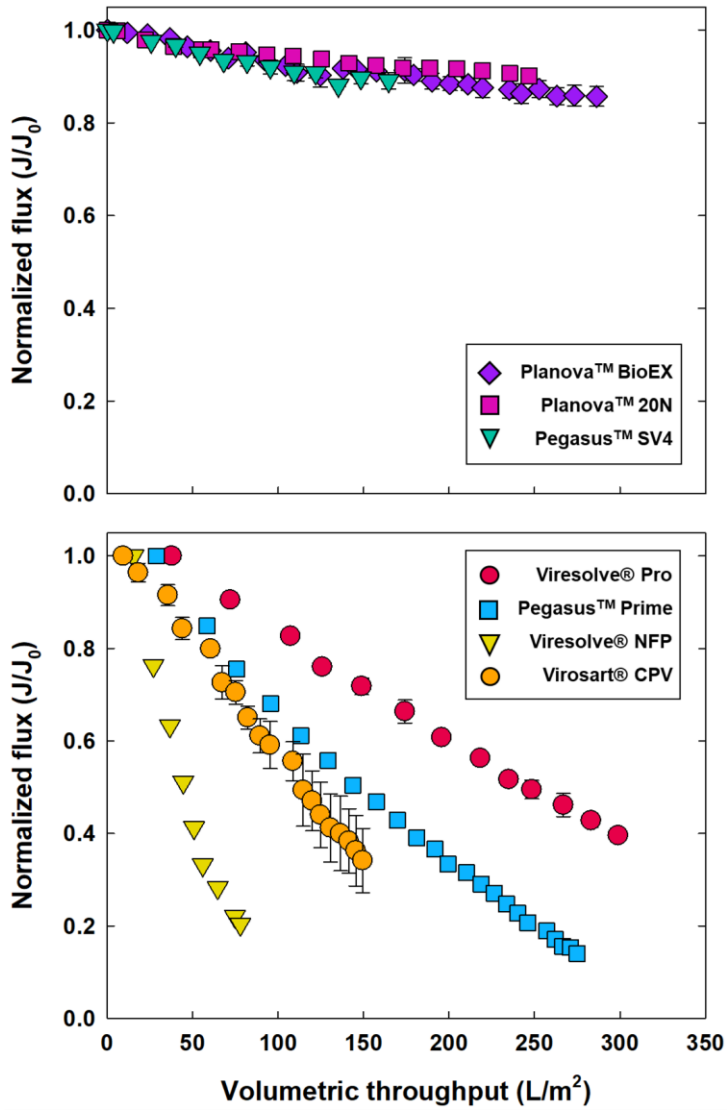

Figure 3-5. Filtrate flux behavior of virus retentive membranes (Planova™ BioEX, Planova™ 20N, and Pegasus™ SV4 (top)) and Viresolve® Pro, Pegasus™ Prime, Viresolve® NFP, and Virosart® CPV (bottom)), presented by normalized flux (J/J_0) as a function of volumetric throughput (L/m^2). Feed solution contained 1 g/L of BSA with ~10^7 PFU/mL of MS2 bacteriophage in 10 mM PBS solution at pH 7.4.

To investigate the flux decay caused by the presence of protein, another set of virus filtration experiments were carried out with ~10^7 PFU/mL MS2 bacteriophage in a 10 mM PBS solution at pH 7.4. In the absence of protein in the solution, flux decay was negligible up to 170 – 300 L/m^2 for all membranes except Viresolve® NFP, which showed 15% flux decay until 300 L/m^2, as shown in **Figure 3-6**. Additionally, initial flux of virus-only solution was almost the same as buffer flux, indicating that the lower initial flux of feed solution containing protein and flux decay were mainly caused by the presence of protein. Severe flux decay of Viresolve® NFP with virus solution could be explained by large pore size gradients (PSGs), as it is made by casting on top of a microfiltration membrane (Fallahianbijan et al., 2019). It is noted that membranes with steep PSGs are more prone to protein fouling (Kosiol et al., 2018). Additionally, the low interconnectivity of Viresolve® NFP near the exit side caused hindrance in flow distribution by virus particles, which were instead captured in virus retentive region (Fallahianbijan et al., 2020). To confirm protein dominant fouling mechanism in virus filtration, Viresolve® Pro membrane was tested without 10^7 PFU/mL MS2 bacteriophage suspension, showed similar flux decline behavior with 10^7 PFU/mL MS2 suspended solution, confirmed protein dominant fouling effect of virus filtration process (data not shown).

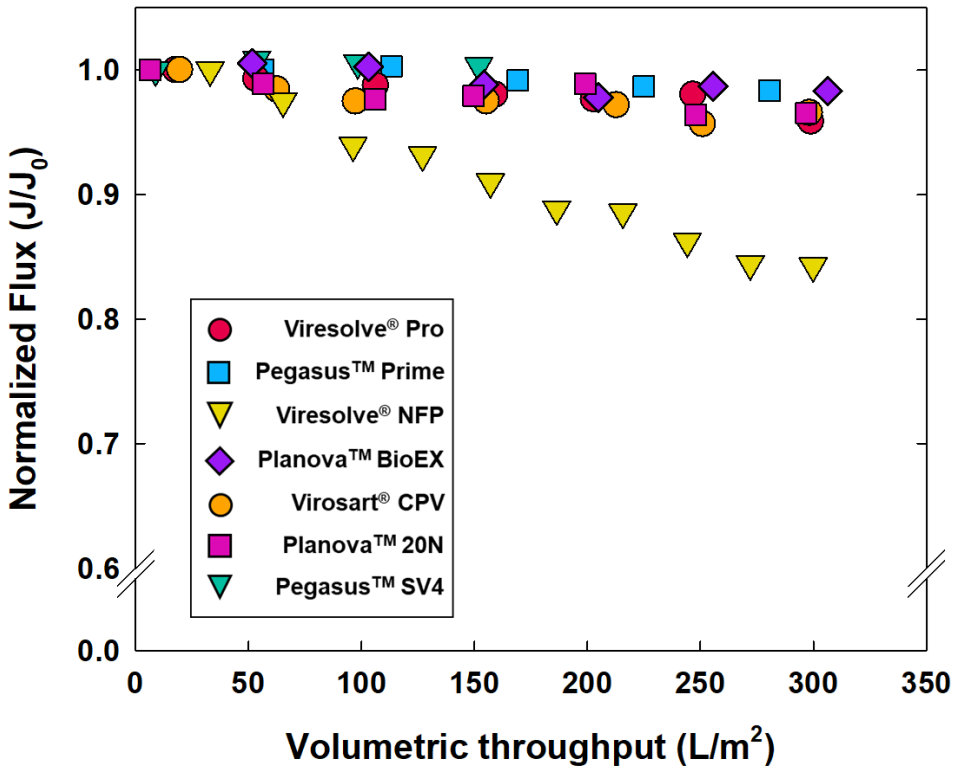

Figure 3-6. Filtrate flux behavior of virus retentive membranes presented by normalized flux (J/J_0) as a function of volumetric throughput (L/m^2). Feed solution contained ~10^7 PFU/mL of MS2 bacteriophage in 10 mM PBS solution at pH 7.4.

Flux decay by membrane fouling could be affected by hydrodynamic conditions, membrane properties, and feed solution compositions (Koo et al., 2012; Marshall et al., 1993). It seemed that the membranes having a relatively higher filtrate flux (e.g., Viresolve® Pro, Pegasus™ Prime, and Viresolve® NFP), might relate to the hydrodynamic drag force. As shown in **Figure 3-7a**, flux decay is plotted as a function of the initial buffer flux. It appears that a higher drag force leads to greater flux decay, although the correlation is not linear (R^2 = 0.56). The higher drag force of the membrane is related to the membrane symmetricity, as asymmetric membranes showed faster buffer flux. Further investigation was approached by categorizing membranes by its polymers (PES or PVDF). As results, the O/C ratio of each material seemed to related protein fouling propensity, as higher O/C ration on the membrane surface showed flux decline for both PES and PVDF membranes (**Figure 3-7b**). The higher O/C ratio showed lower protein fouling tendency with not only membrane materials, but also similar asymmetric structure membranes Viresolve® Pro, Pegasus™ Prime, and Viresolve® NFP. For these membranes, pore size gradients near filtrate side were compared. Viresolve® Pro and Pegasus™ Prime showed 4 – 8 nm/μm increase of pore diameter from membrane exit to upper side, while Viresolve® NFP showed over 16 nm/μm increase, considered as ‘steep’ pore size gradient. The PSG characteristics of Viresolve® NFP showed severe fouling, compared to other asymmetric membranes **(Figure 3-7c)**. This result was consistent with previously reported results that ‘shallow’ pore size gradients showed low flux decline as slow increase of pore size acted as ‘pre-filter’ to protect large molecules deposition near active layer of the membrane (Kosiol et al., 2018). The steep pore size change was critical to fouling propensity regardless of the direction of pore size increase. Unlike other

asymmetric membranes, Virosart® CPV had decreased pore size gradients from membrane exit to upper 6 μm region. The decreased pore size gradients with rapid pore size change caused not only relatively low membrane permeability, but also severe protein fouling compared to other low filtrate flux membranes.

Not only pore size gradients near filtrate side, but also membrane upper region membrane structure was compared between Viresolve® Pro and Pegasus™ Prime membranes. Figure 3-7d shows the SEM images of upper 10 μm cross-section of Viresolve® Pro and Pegasus™ Prime membrens. The membranes had similar pore size gradients near filtrate side, but distinctive fouling behaviors were obtained. As mentioned above, the upper region of Viresolve® Pro showed pore size over 1 μm, acted as effective pre-filter for large molecules or protein aggregates. Pegasus™ Prime, however, obtained upper region pore size of 200 – 300 nm, caused more severe fouling in upper region for faster filtrate flux decline than Viresolve® Pro membrane.

Based on the experimental results of protein fouling of tested membranes and its relationship to membrane properties, it can be concluded that membrane symmetricity, pore size gradients, and higher oxygen content on membrane surface were key three factors to control protein fouling in virus filtration. To clearly investigate membrane symmetricity on protein fouling propensity, Viresolve® Pro and Pegasus™ SV4 membranes were tested under the same hydrodynamic force conditions, as seen in **Figure 3-8**. Regardless of the same hydrodynamic force conditions, Viresolve® Pro membrane showed higher degree of protein fouling compared to Pegasus™ SV4 membrane due to the asymmetric membrane structure with dense active layer near filtrate side.

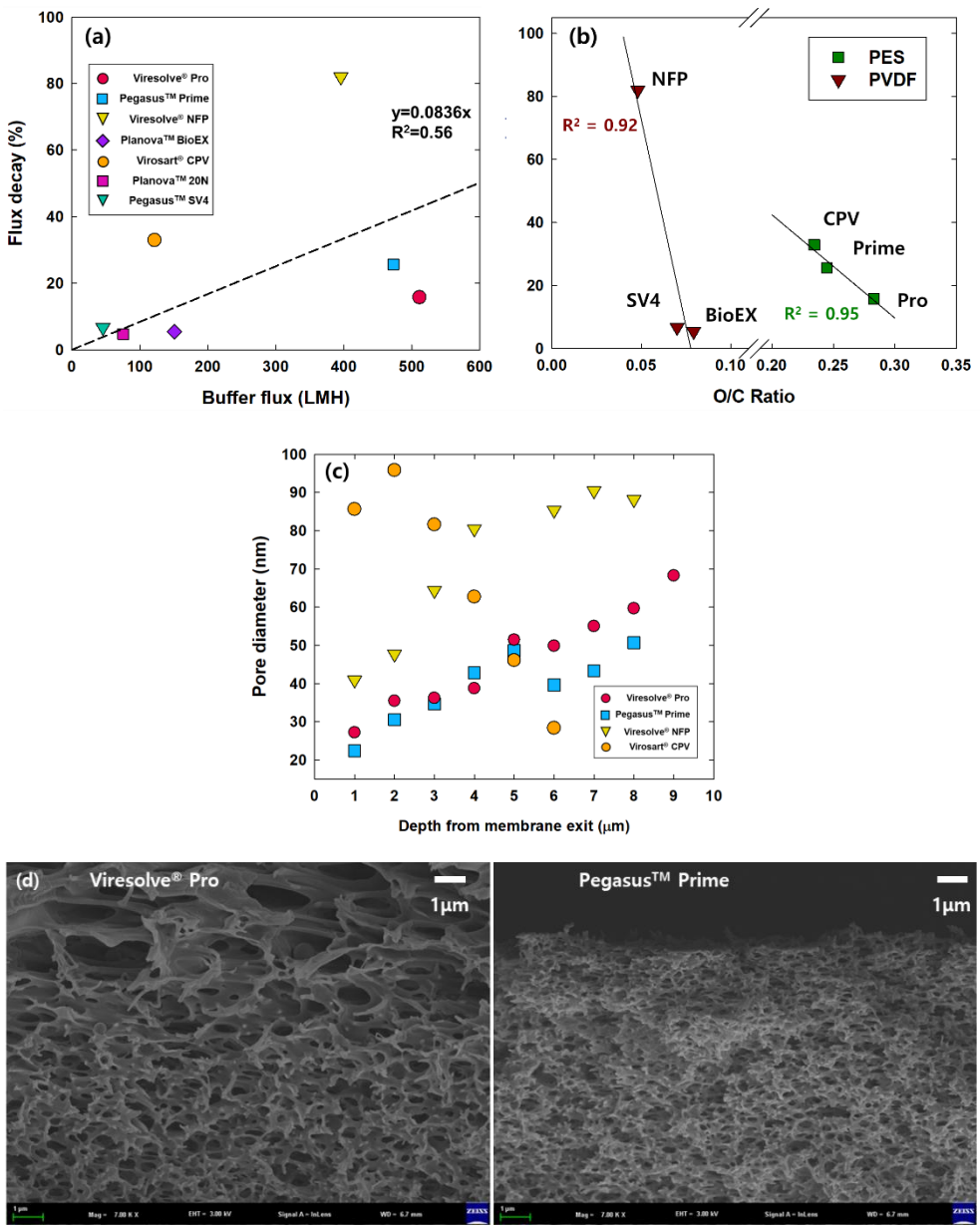

Figure 3-7. (a) Flux decay by 1 g/L BSA vs. pure buffer flux of commercial virus filtration membranes, (b) Flux decay by 1 g/L BSA vs. O/C ratio of membrane surface (c) Pore size gradients comparison between asymmetric membranes and (d) SEM images of upper cross-section of Viresolve® Pro and Pegasus™ Prime.

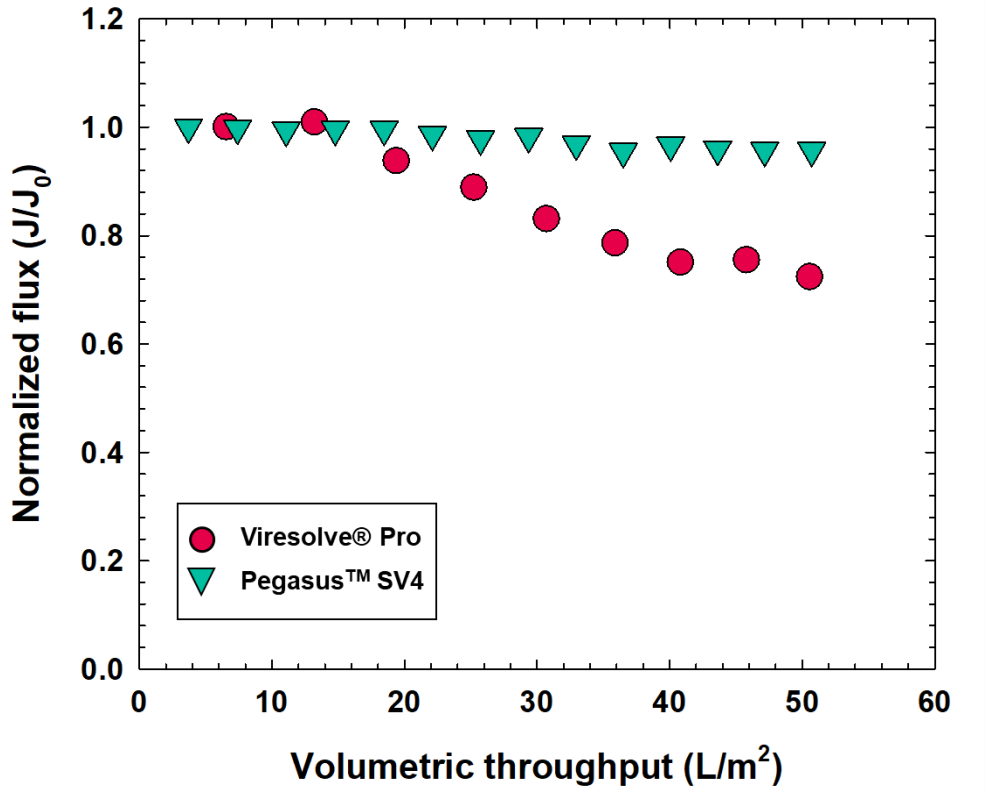

Figure 3-8. Filtrate flux as function of volumetric throughput of Viresolve® Pro and Pegasus™ SV4 under filtrate flux of 50 LMH.

3.3.3. Fouling mechanism difference by membranes

Classical fouling models were introduced to explain various filtrate flux behaviors due to protein fouling in virus-retentive membranes. Initially, double logarithmic plot of d^2t/dv^2 vs. dt/dv was plotted to obtain fouling index from slope value. The values of 0, 1, 1.5, and 2 indicate cake filtration, intermediate blocking, standard blocking (pore constriction) and complete blocking, respectively (Hermia, 1982). The obtained slopes of all membranes indicated complete blocking model (n = 2) as shown in **Figure 3-9**. Although main foulant by complete blocking is assumed to be large oligomers in the BSA solution, seven membranes showed different behavior of the filtrate flux for during BSA fouling, indicated fouling mechanism could be differed by each membrane. Therefore, the most suitable fouling model was determined when the fouling model as a function of filtration time showed the highest correlation with experimental data. Model prediction of each fouling type used the following equations (Iritani & Katagiri, 2016).

$$J_{complete} = J_0 \exp(-k_b t) \quad (3\text{-}2)$$

$$J_{standard} = \frac{J_0}{\left(\frac{k_s J_0}{2} t + 1\right)^2} \quad (3\text{-}3)$$

$$J_{intermediate} = \frac{1}{\left(k_i t + \frac{1}{J_0}\right)} \quad (3\text{-}4)$$

$$J_{cake} = \frac{J_0}{\left(1 + 2k_c J_0^2 t\right)^{\frac{1}{2}}} \quad (3\text{-}5)$$

where J_0 is the initial filtrate flux, k_b, k_s, k_i, k_c are the fouling constants for each model, and t is the filtration time. The highest correlation between experimental data and model calculation was determined by the root mean squared errors (RMSE), calculated as following equation.

$$RMSE = \sqrt{\frac{\sum_{i=1}^{n}(J_{exp}-J_{model})^2}{n}} \quad (3\text{-}6)$$

where J_{exp} is the experimental flux and J_{model} is the flux calculated from the best-fitted model described in equations above. The best-fit fouling model was determined with the lowest RMSE value unless it was similar with others. The best-fit fouling models with 1 g/L of BSA solution were determined as follows: complete blocking model for Viresolve® Pro and Virosart® CPV, standard blocking model for Pegasus™ Prime and Viresolve® NFP. The fouling model for Planova™ BioEX, Planova™ 20N, and Pegasus™ SV4 were unable to be determined due to their less flux decay up to filtration time of 2 – 4 h a/nd similar RMSE values for all fouling models. Consider the smaller size of BSA compared to nominal pore size of virus filtration membranes, the pore constriction (standard blocking) model is seemed to be suitable, as shown for Pegasus™ Prime and Viresolve® NFP. On the other hand, Virosart® CPV which has decreased PSGs from membrane exit caused complete blocking by not only large oligomers of BSA, but also smaller dimers of BSA near upper 5 – 6 μm region from the exit side.

The protein fouling mechanism was further confirmed by CLSM cross-section images of Viresolve® Pro and Pegasus™ SV4 membranes by fluorescently labeled albumin filtration **(Figure 3-10)**. As seen inf **Figure 3-10**, different fouling regions were observed. Viresolve® Pro showed majority of protein blocking near filtrate side, where small pores are distributed densely. In contrast, protein deposition behavior Pegasus™ SV4 showed that most of protein deposited near the top surface. The protein fouling visualization confirmed that significant pore blocking caused filtrate flux decline for Viresolve® Pro membrane and cake layer formation of Pegasus™ SV4, although the flux decline of Pegasus™ SV4 was insignificant.

The different fouling mechanism by membrane structures suggest the importance of membrane structure since the structural properties determine not only the filtrate flux decline behaviors, but also the different fouling mechanism occur under the same feed solution compositions. Recently, combined complete pore blocking and cake filtration fouling mechanism by 1 g/L human IgG fouling was proposed (Peles, Fallahianbijan, et al., 2022), suggested that actual fouling phenomenon during virus filtration is complicated.

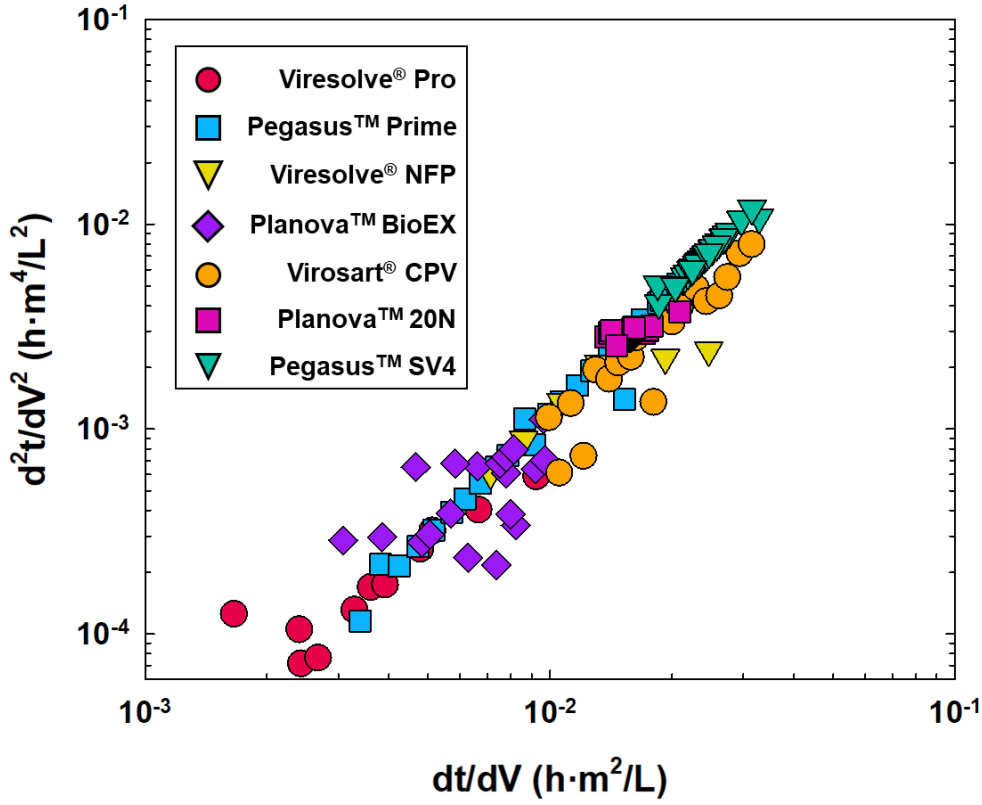

Figure 3-9. Fouling index prediction plot (d^2t/dV^2 vs. dt/dV) for 1 g/L of BSA and ~10^7 PFU/mL of MS2 bacteriophage in 10 mM PBS at pH 7.4.

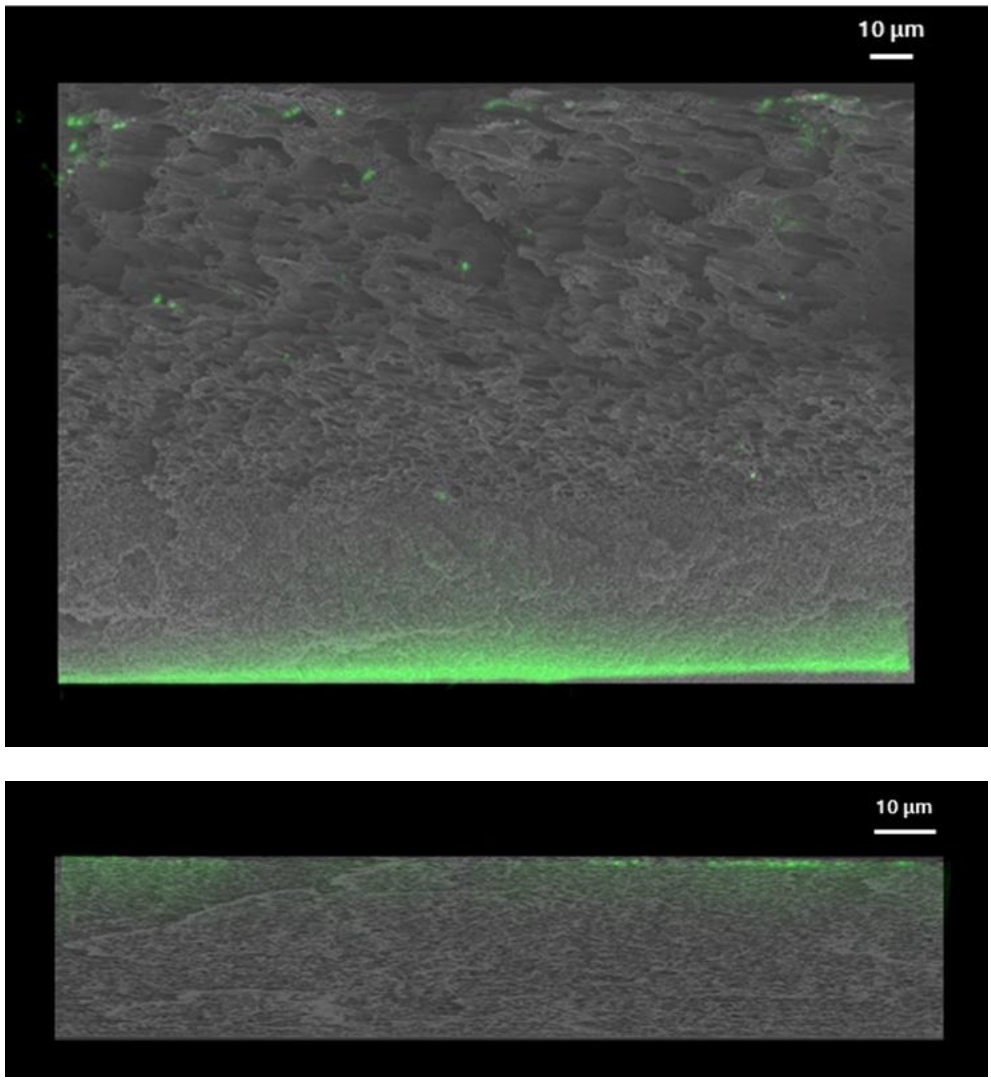

Figure 3-10. CLSM cross-section images of fluorescently labeled albumin filtered membranes. Top: Viresolve® Pro and bottom: Pegasus™ SV4.

3.3.4. Virus breakthrough behavior comparison

Figure 3-11 shows the virus breakthrough behavior, presented as LRV change, as a function of volumetric throughput under 1 g/L BSA with 10^7 PFU/mL MS2 bacteriophage solution. No virus breakthrough was observed for most membranes until 150 – 300 L/m^2 except for Viresolve® NFP and Pegasus™ SV4. LRV decreased to 1.2 and 4.5 for Viresolve® NFP until 80 L/m^2 and Pegasus™ SV4 until 170 L/m^2, respectively. Viresolve® NFP demonstrated the most severe flux decay and virus breakthrough. It is noticed that only the LRV performance of Viresolve® NFP is linearly related to the filtrate flux (Bolton et al., 2005). The flux decay dependent LRV reduction indicates that possible foulants (i.e., viruses or proteins) could inhibit virus retention and cause virus breakthrough. On the other hand, Pegasus™ SV4 showed some virus breakthrough but less flux decay, indicating that protein fouling propensity is not directly related to the virus breakthrough behavior. Instead, both membranes have relatively large nominal pore diameters, which largely affects LRV performance (Kosiol et al., 2017). Similar behavior of virus breakthrough for both membranes was also observed in the absence of protein in the solution, which presented less LRV reduction on the right at **Figure 3-11**. It appeared that the presence of proteins could affect to virus breakthrough behavior in some cases.

Additional experiments were performed to evaluate the effects of virus size on filtrate flux and virus breakthrough behaviors, as shown in **Figure 3-12**. Data was obtained from similar virus filtration using Viresolve® NFP and Pegasus™ SV4 with bacteriophage PP7, which is known to be slightly larger than bacteriophage MS2 (Tars et al., 2000). Interestingly, no virus breakthrough was observed for Pegasus™ SV4, while virus breakthrough behaviors for Viresolve® NFP are

similar as the same titer of MS2 filtration. Note that the nominal pore size of Pegasus™ SV4 was slightly larger (i.e., 33.2 nm) than that of PP7, and that of Viresolve® NFP was much larger (i.e., 45.9 nm). Only a few nanometers of difference appear to have a significant impact on virus breakthrough behavior.

Figure 3-13 shows the nominal pore size comparison between SEM image analysis and GLP pore size measurement. The SEM image seemed overpredict the nominal pore diameter of membranes due to the images were taken under dry state. Also, the pore diameter was measured by assuming pore shapes were circular, while most of virus filtration membranes had non-circular pore shape. However, the GLP data correlated with SEM pore diameter measurement, where slightly larger nominal pore size detection of Viresolve® NFP and Pegasus™ SV4 membrane. Not only larger nominal pore size, but also, pore diameter detection of ~ 30 nm were detected for both Viresolve® NFP and Pegasus™ SV4 membrane, caused undesired virus breakthrough by 10^7 PFU/mL MS2 bacteriophage filtration.

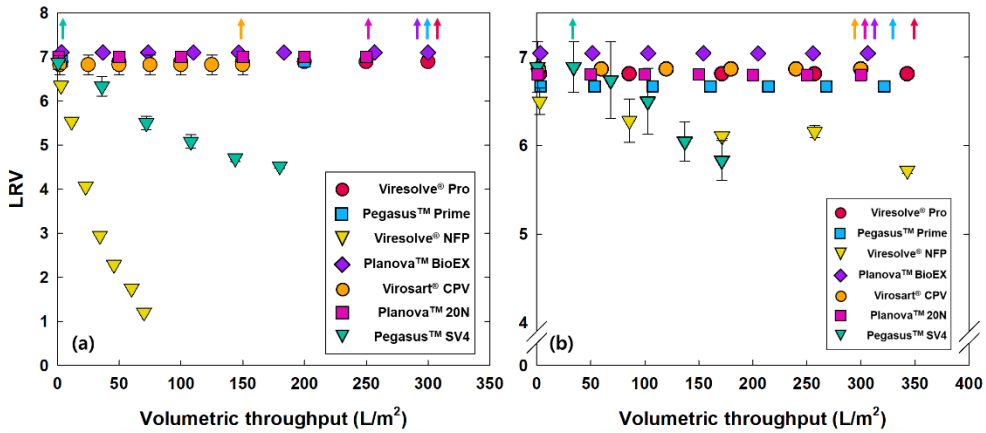

Figure 3-11. Left: log reduction value (LRV) as function of volumetric throughput feed solution with 1 g/L of BSA and 10^7 PFU/mL MS2 bacteriophage in 10 mM PBS Right: 10^7 PFU/mL MS2 only in 10 mM PBS. Upper arrows indicated no phage detection in filtrate up to the volumetric throughput where arrows placed.

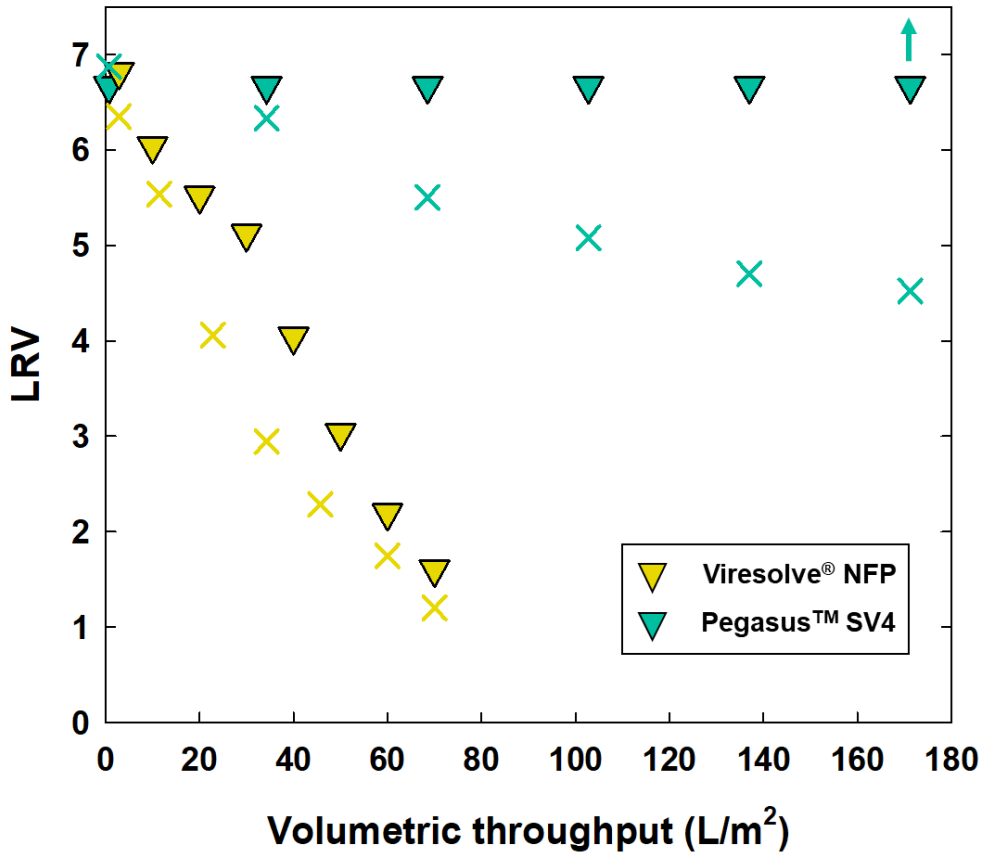

Figure 3-12. Log reduction value (LRV) as function of volumetric throughput of Viresolve® NFP and Pegasus™ SV4 with 1 g/L BSA and 10^7 PFU/mL of PP7 bacteriophage in 10 mM PBS solution, in comparison with LRV of 10^7 PFU/mL of MS2 bacteriophage (x marks).

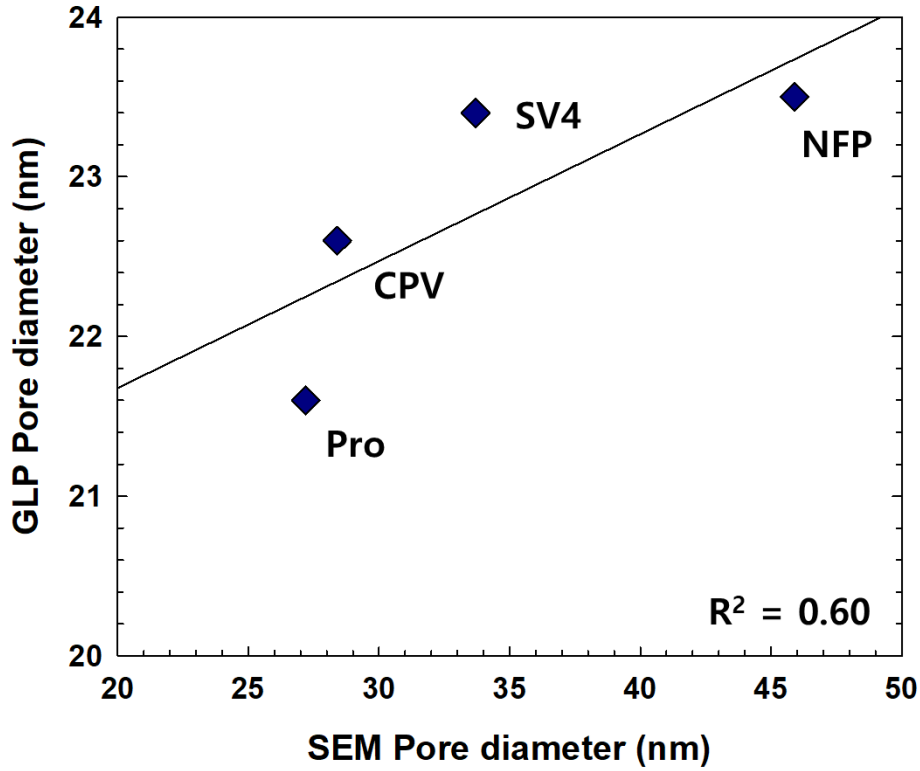

Figure 3-13. Pore size measurement correlation between SEM images and GLP analysis.

3.3.5. Effect of protein concentration on filtration performance

Figure 3-14a and **Figure 3-14b** shows filtrate flux and virus breakthrough behaviors as functions of volumetric throughput by using 5, 10, and 20 g/L of BSA with ~10^7 PFU/mL MS2 bacteriophage in PBS solution. Viresolve® Pro and Pegasus™ SV4 were selected due to different protein fouling propensities and membrane morphology. Initial filtrate fluxes for Viresolve® Pro decreased from 346.7 LMH to 242.6 LMH due to increased BSA concentration, while those for Pegasus™ SV4 were similar at 40.5 – 41.5 LMH due to a much lower drag force. Higher drag force for Viresolve® Pro increased the effect of concentration polarization and possibly accumulated more proteins during the initial flux measurement. On the other hand, these effects became insignificant for Pegasus™ SV4 due to lower initial flux.

Interestingly, the best-fitted fouling model for Viresolve® Pro was changed to the standard blocking at higher protein concentration with showing the lowest RMSE value (**Table 3-5**). Viresolve® Pro had shallow PSGs from membrane exit with high interconnectivity (Brickey et al., 2021; Fallahianbijan et al., 2020) where relatively lower contents of large oligomers dominantly blocked the pores (i.e. complete blocking) at 1 g/L of BSA solution while relatively smaller BSA with large contents (>75%) at higher protein concentration condition would mainly clogged the pores, resulted in the changed the model to standard blocking. On the other hand, RMSE of all fouling models for Pegasus™ SV4 showed similar value regardless of protein concentration, with the closest model could be cake filtration.

The virus breakthrough, presented in **Figure 3-14c** and **Figure 3-14d**, deteriorated with increased protein concentration. In the case of Viresolve® Pro, there was no detection of bacteriophage until 300 L/m^2, corresponding to 300 g/m^2

of protein mass throughput with 1 g/L of BSA. However, visible plaques were found in filtrate samples at higher BSA concentrations. Viresolve® PRO showed the first phage detection at approximately 300 g/m^2. On the other hand, initial virus breakthrough was observed with Pegasus™ SV4 at 10 g/L and 20 g/L of BSA concentration due to relatively larger pore diameter. It seems that high protein concentration may cause earlier virus breakthrough during filtration, potentially leading to a failure in viral clearance. In addition, Viresolve® Pro seemed to be lower virus breakthrough due to its narrow pore size distribution.

In order to clearly define the phenomenon of virus breakthrough in both membranes, a pre-fouling experiment was performed by 10 g/L BSA filtration up to 30 L/m^2 and then ~10^7 PFU/mL of MS2 bacteriophage solution was filtered up to the similar throughput as protein added. As shown in **Figure 3-15**, results showed higher virus retention under pre-fouling conditions for both membranes, indicating neither filtrate flux decline nor certain protein mass loading was responsible for virus breakthrough; the high concentration of protein inhibited the virus retention selectivity during filtration. When the protein and virus were co-mixed in the buffer, this caused undesired breakthrough. The different virus removal performances between virus filtration after protein fouling and virus-protein co-suspended solutions suggest that the solution complexity affects virus removal, regardless of the structural differences.

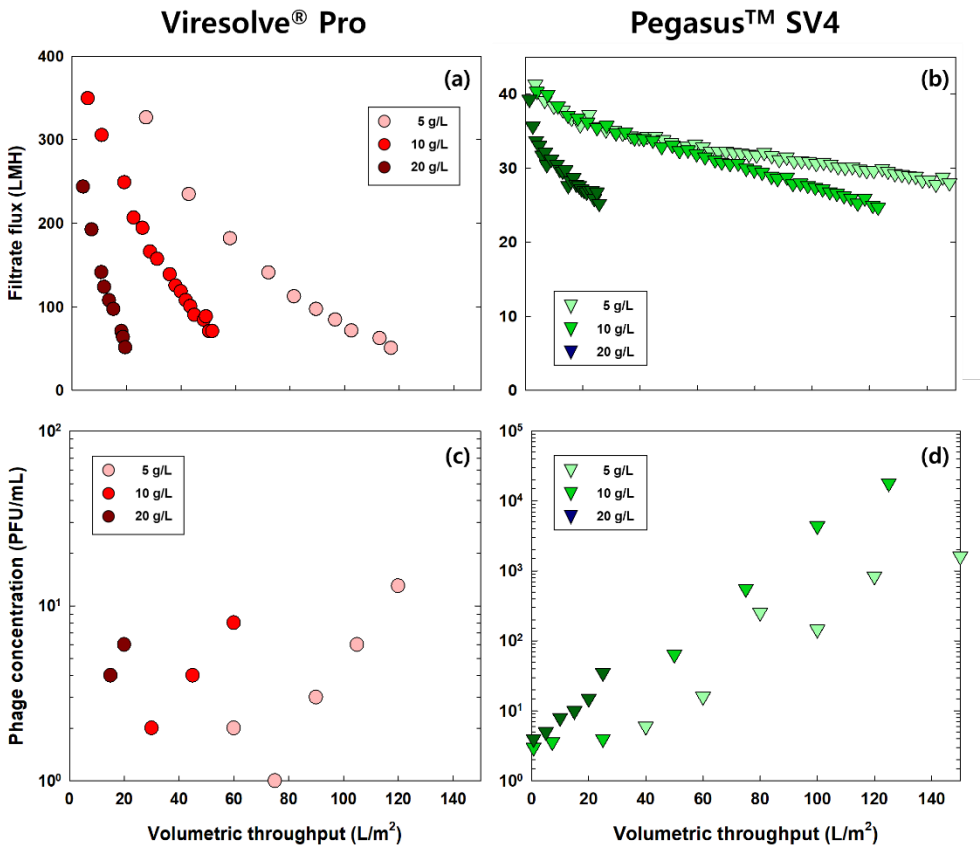

Figure 3-14. Filtrate flux (a and b) and virus breakthrough (c and d) behavior of Viresolve® Pro and Pegasus™ SV4 membranes, under 5, 10 and 20 g/L BSA with 10^7 PFU/mL MS2 bacteriophage in 10 mM PBS solution, as function of volumetric throughput increase.

. **Table 3-5.** RMSE of Viresolve® Pro and Pegasus™ SV4 membranes during virus filtration with 5, 10 and 20 g/L of BSA solution. The lowest RMSE was assumed to the most suitable fouling model.

	Protein conc. (g/L)	Complete blocking	Standard blocking	Intermediate blocking	Cake filtration
Viresolve® Pro	**5**	10.1	7.5	21.1	41.5
	10	10.4	3.9	14.8	33.8
	20	6.0	2.8	10.0	21.9
Pegasus™ SV4	**5**	2.8	2.6	2.4	2.0
	10	0.8	0.6	0.5	0.4
	20	4.1	3.4	2.9	2.0

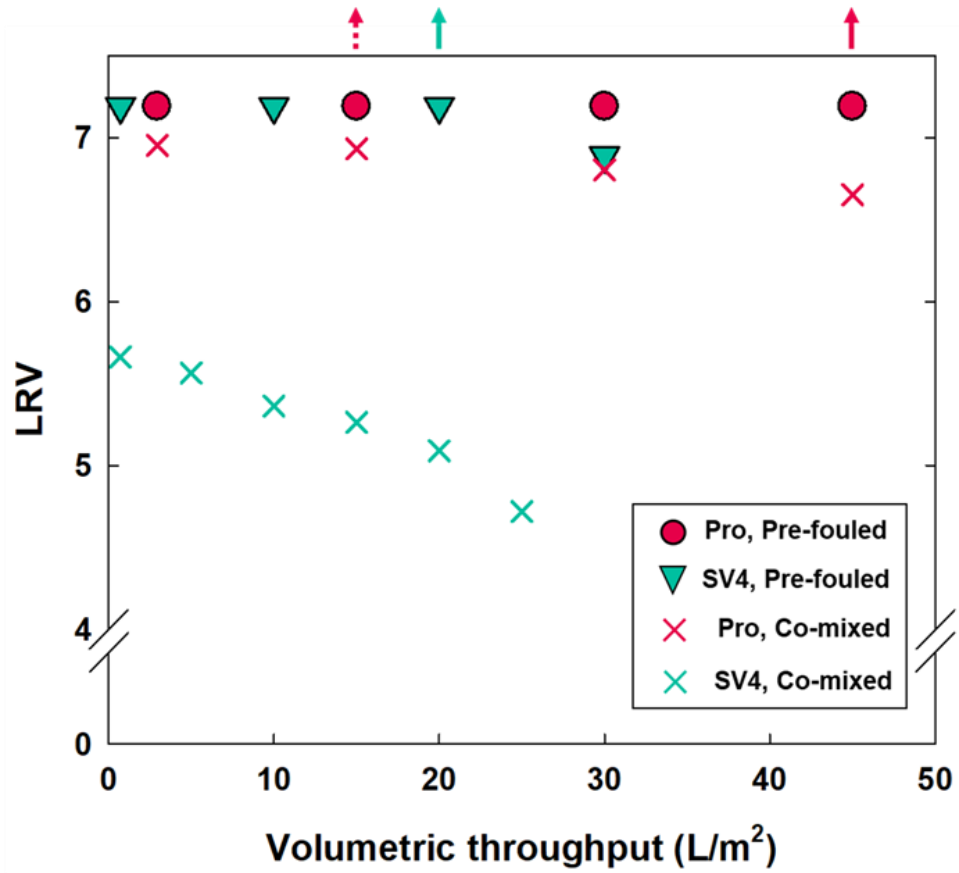

Figure 3-15. LRV as a function of volumetric throughput for pre-fouling experiment using Viresolve® Pro and Pegasus™ SV4 membranes. Feed solution contained 10 g/L of BSA with ~10^7 PFU/mL MS2 bacteriophage in 10 mM PBS solution. x marks from LRV were obtained data from **Figure 3-11**.

3.4. Summary

In this chapter, the effect of protein fouling on filtrate flux decline and virus breakthrough behaviors were investigated using seven different commercially available small-virus removal membranes. This study aimed to define relationship between membrane properties and its impact on filtration performance. As results, membrane symmetricity contributed to determine membrane permeability, as asymmetric structure membranes showed higher permeability than relatively symmetric membranes, prone to fast filtrate flux decline by protein filtration. For asymmetric membranes, pore size gradients near filtrate were important factor to determine protein fouling propensity, as increased pore size gradients with low pore size increase showed less fouling propensity due to actively remove large molecules near filtrate side. Not only structural properties, but also higher oxygen component caused lower fouling propensity. In terms of virus removal performance, most of membranes maintained LRV over 7 up to 300 L/m^2 with or without presence of protein in feed solution. Membranes with broader PSDs with >25nm pore detection was responsible for undesired virus breakthrough.

4. Virus breakthrough behaviors under various feed solution compositions and operating conditions

4.1. Introduction

Viral contamination from mammalian cell-based bioproducts has been critical concern for the biotechnology industry (Ajayi, Johnson, Faison, Azer, Jackie, et al., 2022). Current regulation for viral safety requires validation of viral safety from raw materials, during downstream process, and final products (ICH, 2022). To ensure viral safety, downstream process includes at least two viral clearance processes, such as viral inactivation and virus filtration (Shukla & Aranha, 2015). Virus filtration process, polymer-based membrane filtration process for virus removal, is considered as key unit operation to ensure viral safety from both adventitious and endogenous viruses (Johnson et al., 2022). In particular, the worst-case scenario virus in mammalian-cell derived products, murine minute virus (MMV) from Chinese hamster ovary (CHO) cell can be effectively removed by virus filtration process (Gefroh et al., 2014). The nominal pore size of virus filtration membrane is approximately 20 nm for effective removal of virus with high transmission of biopharmaceuticals (Roth et al., 2020).

The main removal mechanism of virus filtration membrane is size exclusion, where virus is ‘captured’ in virus retentive region of the membrane, similar to the depth filters (Nejatishahidein & Zydney, 2021). Therefore, the membrane morphology is considered as key factor determining virus removal performance. For membranes with homogeneous structure, the virus removal mechanism and its modeling were well-established. Jackson et al. proposed the internal concentration polarization model, the “free” virus accumulation near membrane surface caused

overchallenge of virus particles near membrane surface, resulted as undesired virus breakthrough (Jackson et al., 2014). For asymmetric structure membranes, virus removal mechanisms have been explained by visualizing the retention behaviors of viruses or representative virus surrogates such as nanoparticles or bacteriophages (Fallahianbijan et al., 2017; Leisi et al., 2021). Leisi et al. reported that asymmetric membranes were less prone to virus particle attenuation due to dense rejection layer acted as barrier of virus breakthrough (Leisi et al., 2021). Recent study showed structural difference between homogenous Pegasus™ SV4 virus filter and highly asymmetric Viresolve® Pro membrane by focused-ion beam scanning electron microscopy (FIB-SEM) (Russell et al., 2023), showed highly accurate pore structure difference and the different nanoparticle retention performances.

Previous studies well established the robust virus retention mechanism of virus filtration membranes, and the risk of undesired virus breakthrough under certain process condition was reported, such as flow interruption (Dishari, Venkiteshwaran, et al., 2015) and low filtrate flux operation (Fan et al., 2021; Yamamoto et al., 2014). Flow interruption mostly occurred during post buffer flush for product recovery (LaCasse et al., 2016), while low filtrate flux operation is aimed to adopt virus filtration process in continuous downstream process (Zydney, 2016). The main reason of virus breakthrough via flow interruption or low flux filtration was considered to be increase of virus diffusion force, which enabled the passage of virus through the interconnected pore structure (Yamamoto et al., 2014). The diffusive dominant flow rate can be determined by the Peclet number, where the Peclet number is less than 1 is considered as the diffusive force dominant flow condition. Previous study reported that the effective virus diffusivity in membrane substrate is approximately two orders of magnitude lower, equivalent diffusive

force dominant flow of MMV was to be approximately 36 LMH (Fan et al., 2021).

The objective of this study was to determine virus breakthrough point under various conditions, such as overchallenged virus per unit membrane area, high protein concentration, flow interruption and low flux filtration. The main results determined robust virus retention capacity up to 10^{12} PFU/m^2 for model virus surrogate, without protein interruption or flow conditions. The effect of protein, flow interruption, and low filtrate flux were investigated, suggest safe virus filtration operation for current and future downstream process.

4.2. Materials and methods

4.2.1. Materials

The Viresolve® Pro micro 40 devices (VPMKVALNB9) from EMD Millipore Corporation (Bedford, MA, USA) was used for virus filtration experiments. The device consists of two layers of Virsolve® Pro membrane, packed as syringe module with an effective membrane area of 3.4 cm^2. *Pseudomonas aeruginosa* bacteriophage PP7 (ATCC-15692-B4) and *Escherichia coli* (*E. coli*) bacteriophage MS2 (ATCC-15597-B1), purchased from the American Type Culture Collection (ATCC®, USA), were used as small virus surrogates. For most of experiments, bacteriophage PP7 was used, as commonly used virus surrogate in previous studies (Jackson et al., 2014; Kosiol et al., 2019). Bacteriophage propagation and purification procedure was followed by ATCC® product sheet (Adams, 1959). Briefly, single cell was cultured in appropriate nutrient media for 18 h at 37℃, then 200 μL of a high phage titer stock was spiked into host cell and stored overnight in 37℃ without agitation. The phage suspended solution was purified via centrifugation at 3,000 × g for three times for collect the supernatant. The supernatant was further purified by 0.2 μm filtration to remove residual cell debris and undesired particulates. The phage stock was stored in 4℃ in prior to use in filtration experiments.

Bioperformance-certified phosphate buffer saline (PBS, P5368; Merck, USA) was used as the model buffer solution. 1 pouch of power equivalents with 10 mM phosphate buffer containing 137 mM NaCl and 2.7 mM KCl at pH of 7.4. Bovine serum albumin (BSA, A7906; Merck, USA) was selected as the model protein.

4.2.2. Virus filtration process

Virus filtration was performed under constant pressure with N_2 gas purging with applied pressure of 2 bar, close to manufacturer's suggested operating pressure. In prior to virus filtration, buffer flux was measured with pure buffer solution over 50 L/m^2 for membrane wetting and flux stabilization. Once pure buffer flux is measured, the feed solution was switched to either virus suspended solution or virus and protein suspended solution for virus filtration. Depend on virus titer and protein concentration, the volumetric throughput for each experiment was varied from 50 – 300 L/m^2. Buffer flush experiment was performed after constant pressure filtration of protein suspended solutions, with flow interruption of 10 min. To minimize effect of remained protein and virus in feed tank, PBS solution was filled in different reservoir, connected perpendicularly placed inlet of Viresolve® Pro device. During buffer flush, feed solution inlet was closed to make sure no flow distribution of buffer in feed solution tank. For low flux experiments, filtration was operated as constant flow rate mode by using a peristaltic pump (Gilson). The pump speed was adjusted to maintain 10 LMH. The virus filtration was performed for 6 h, approximately 60 L/m^2 of total filtration. The phage titer and protein concentration were varied in range of 10^4 – 10^9 PFU/mL and 10 – 20 g/L for phage titer and protein concentration, respectively. The filtrate flux was measured by weight change of filtrate volume as filtration time, expressed as LMH. **Figure 4-1 and Figure 4-2** show the experimental scheme of buffer flush and low filtration flux experiments.

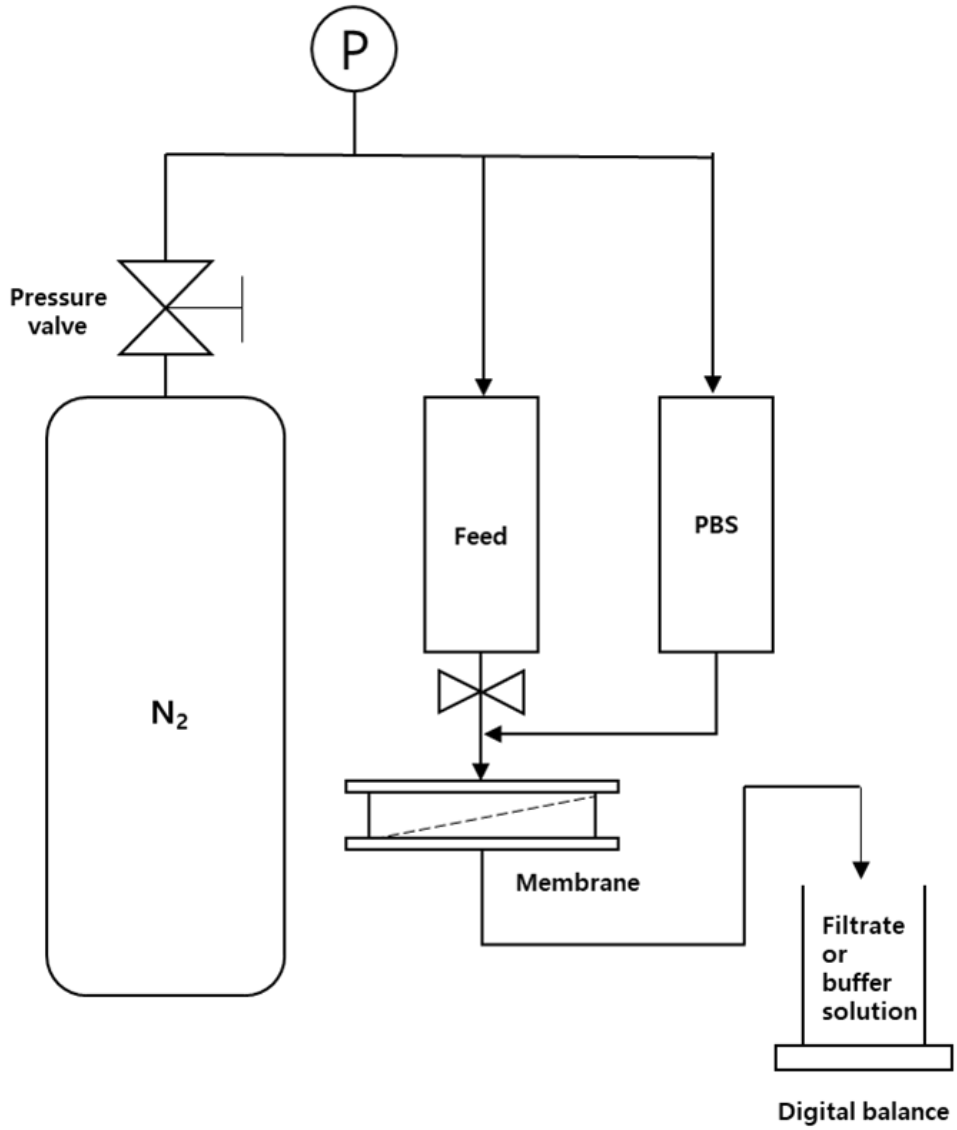

Figure 4-1. Process scheme of post-buffer flush after virus filtration. Once feed solution was filtered, the feed solution valve was closed with 10 min of process pause (pressure-release). After process pause, pure PBS solution was filtered.

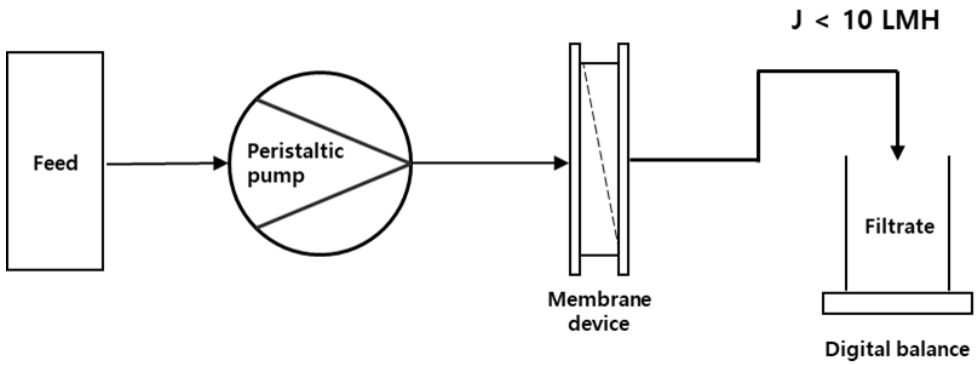

Figure 4-2. Process scheme of low flux filtration experiments.

4.2.3. Analysis

Phage titer was evaluated by plaque forming assay using double-layer agar plate counting. Feed and filtrate samples were mixed with 200 μL of host cell and mixed into 47℃ media containing 0.5% agar solution. The mixture was poured directly into the pre-warmed solidified bottom agar. The clear dots appeared after 6 – 8 h incubation at 37℃. For high titer solutions, serial 10-fold dilution was performed to maintain no more than 10^3 PFU/mL. The virus removal performance was expressed either phage concentration in filtrate solution or log-reduction value (LRV) of virus titer, expressed as following equation (4-1).

$$LRV = -log_{10}(\frac{C_{filtrate}}{C_{feed}}) \quad (4\text{-}1)$$

where $C_{filtrate}$ and C_{feed} are phage titer in filtrate and feed, respectively. Protein concentration was measured by UV-vis absorbance at 280 nm.

4.3. Results and discussion

4.3.1. Virus breakthrough under high phage titer

Figure 4-3 shows the LRV as function of volumetric throughput and phage titer in filtrate as function of virus challenged on membrane, under phage titer conditions of 10^7, 10^8, and 10^9 PFU/mL. To examine virus breakthrough phenomena under various operating and feed solution conditions, Viresolve® Pro membrane was chosen as a model membrane since the membrane is known to provide robust virus removal performance (up to 6-$\log_{10}$ reduction for various small viruses and surrogates); however, the study regarding virus removal performance was limited. Regardless of high viral loading conditions, LRV over 6 was maintained up to 200 - 300 L/m^2, confirmed robust virus removal performance of Viresolve® Pro membrane as double-layered composition. Under 10^7 PFU/mL of PP7 in 10 mM PBS filtration, no phage detection was observed in filtrate up to 300 L/m^2, equivalent to 3.0 x 10^{12} PFU/m^2 of phage challenged on membrane. Under 10^8 and 10^9 PFU/mL PP7 titer conditions, however, the visible phage was observed in filtrate samples. In case of 10^8 PFU/mL filtration, phage started escape through the double layers of Viresolve® Pro membrane at virus loading equivalent to 2 x 10^{13} PFU/mL. 10^9 PFU/mL filtration showed phage detection of initial 3 L/m^2 samples.

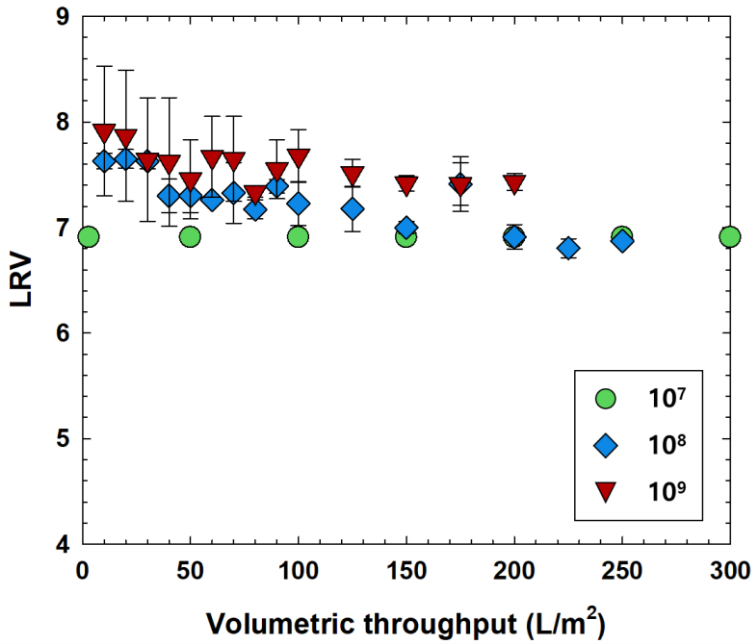

Figure 4-3. LRV as function of volumetric throughput of PP7 bacteriophage under 10^7, 10^8, and 10^9 PFU/mL phage titer.

Figure 4-4 represents the filtrate flux and phage passage profiles comparison of PP7 and MS2 bacteriophage, as function of phage challenged on membrane. MS2 bacteriophage was known to the worst-case scenario virus surrogate for small virus, due to smaller size and low isoelectric point (Langlet et al., 2009). The results showed not only phage breakthrough, but also noticeable flux declines were observed under 10^8 and 10^9 PFU/mL filtrations, where 10^7 PFU/mL filtration showed negligible flux decay up to 3 x 10^{12} PFU/m^2. The flux decline by virus only solution indicated virus particles not only constricted in virus retentive regions, but also redirected to membrane flow path by over challenged phage. The non-constricted virus particles became mobilized in membrane, caused undesired breakthrough once virus diffused through relatively larger pores (Bolton et al., 2005; Yamamoto et al., 2014). However, the nonlinear relationship between phage breakthrough as function of filtrate flux decline (or volumetric throughput) indicated the undesired virus breakthrough was possibly due to the uneven distribution of virus particles to virus retentive region by over challenged phage titer. Viresolve® Pro membrane had structural properties of asymmetric and interconnected structure (Brickey et al., 2021), with broad retention distribution of 20 nm fluorescently labeled nanoparticles and model virus surrogates (Dishari, Venkiteshwaran, et al., 2015; Fallahianbijan et al., 2017). In case of MS2 bacteriophage, less prone to flux decline, but more phage breakthrough under 10^9 PFU/mL filtration. Regardless of the phage type, both virus surrogates showed robust removal performance up to 10^{12} PFU/m^2. It seemed that phage challenge per unit membrane area over 10^{12} PFU/m^2 was responsible for undesired virus breakthrough. For 10^9 PFU/mL filtrations, the fouling mechanism was close to the cake filtration behavior (**Figure 4-5**) for both PP7 and MS2 bacteriophage

filtrations. In case of high phage challenge per unit membrane area, rapid flux decline from initial stage of filtration acted as constriction of not only virus retentive region, but also increased membrane resistance by cake layer formation, caused severe flow path blocking, as well as mitigating virus breakthrough by cake resistance.

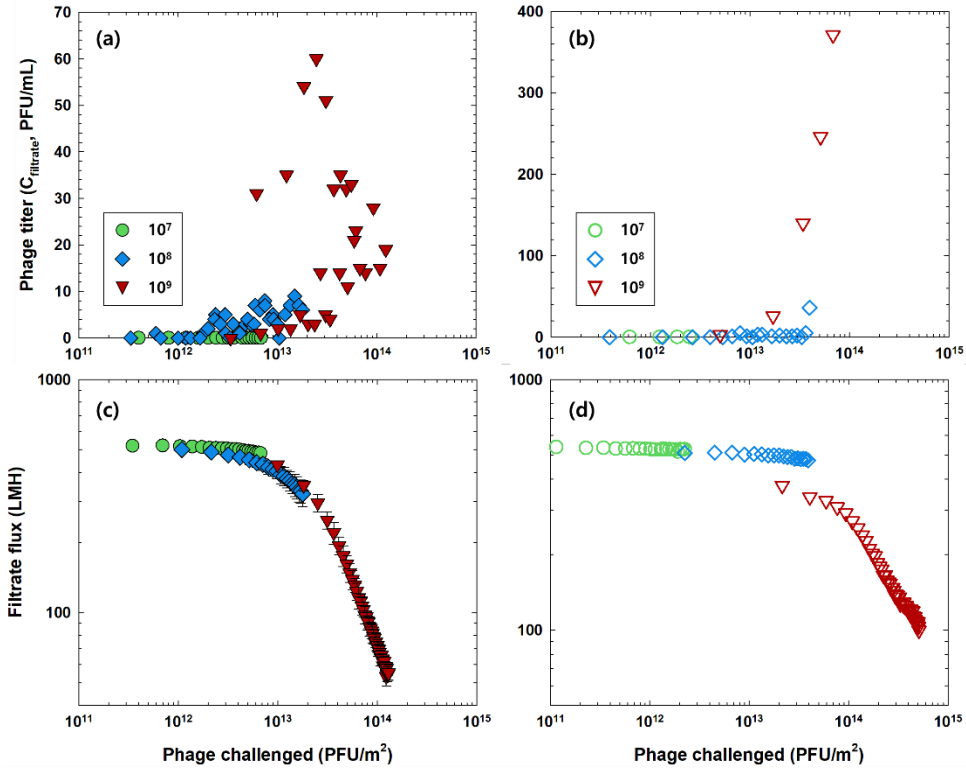

Figure 4-4. Phage breakthrough and filtrate flux profile of bacteriophage PP7 (a and c) and MS2 (b and d).

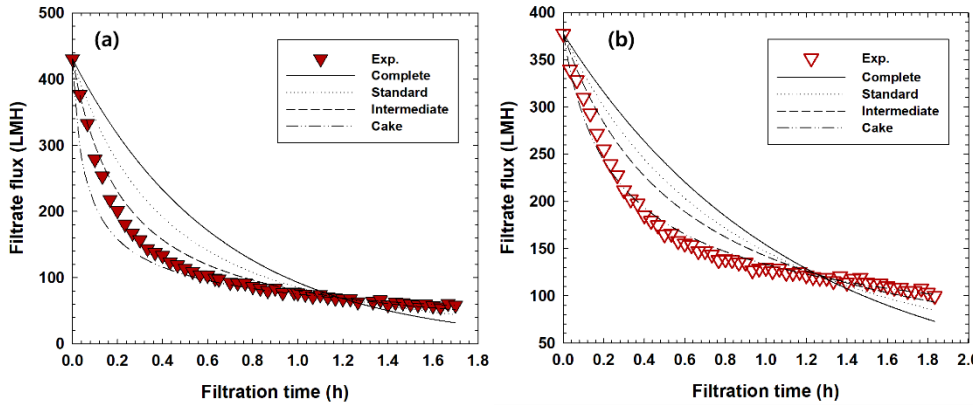

Figure 4-5. Membrane fouling model prediction of 10^9 PFU/mL phage filtration (a) PP7 and (b) MS2

4.3.2. Phage breakthrough by high protein concentration

Figure 4-6 shows the PP7 phage breakthrough profile as function of volumetric throughput, under 10^9 PFU/mL PP7 titer with protein concentrations of 10 and 20 g/L. 10^9 PFU/mL of PP7 phage was chosen as phage titer due to definite phage breakthrough was observed under phage only filtration. The co-mixed condition of high phage titer with 10 and 20 g/L of BSA caused rapid flux decline, over 90% flux decline in volumetric throughput of 50 – 60 L/m^2 (data not shown). Up to 60 L/m^2, 10^9 PFU/mL PP7 only condition showed average phage breakthrough of 18 ± 14.5 PFU/mL; in presence of protein, the phage breakthrough under 10 g/L and 20 g/L were 415 PFU/mL and 1125 PFU/mL at 60 L/m^2 and 57 L/m^2, respectively. The phage titer in filtrate samples showed relatively linear correlation with BSA mass throughput (**Figure 4-7**), indicated simultaneous BSA transmission with phage retention caused loss of phage retention selectivity. Under 10 g/L and 20 g/L, the critical volumetric throughput where LRV <4 was expected as 135 and 91 L/m^2, respectively. To reach the critical volumetric throughput, expected viral challenge on membrane equivalents over 10^{14} PFU/m^2, which rarely occur under real virus filtration process. The main results suggest that potential risk of undesired virus breakthrough under high virus titer with virus retention interruption of protein could threaten the overall viral safety of biopharmaceutical manufacturing. Thus, defining maximum capacity of virus challenge on membrane could be attributed to safe and efficient process operation for virus filtration.

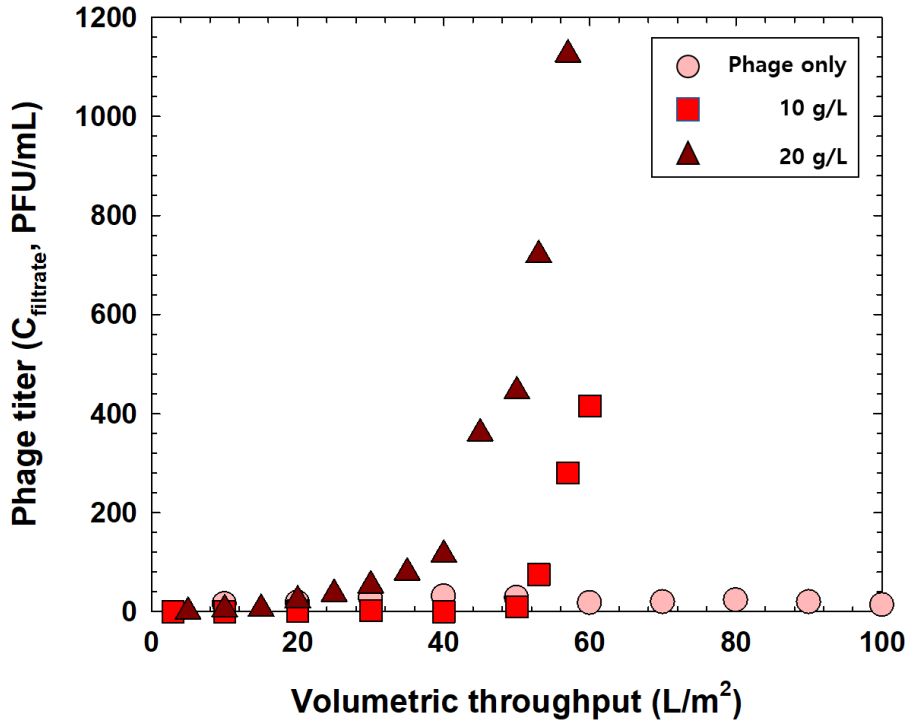

Figure 4-6. Phage titer in the filtrate samples as a function of volumetric throughput. Feed solution of ~ 10^9 PFU/mL of PP7 with 10 and 20 g/L of BSA in 10 mM PBS solution was used.

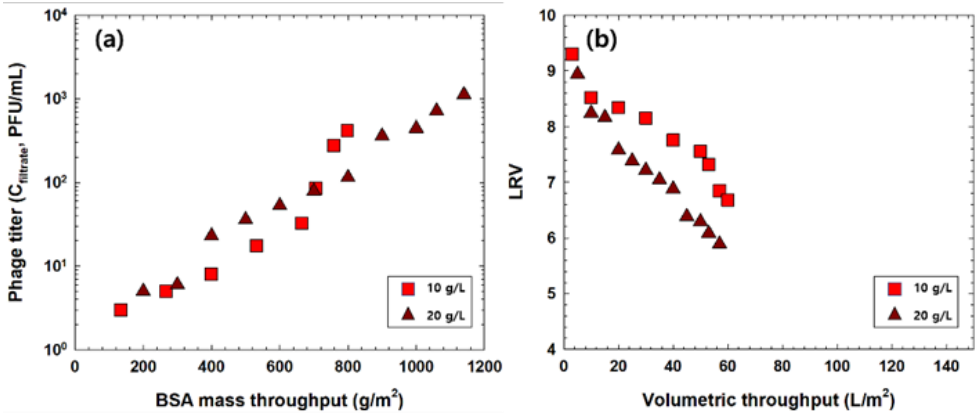

Figure 4-7. (a) LRV as function of volumetric throughput and (phage breakthrough profile as function of BSA mass throughput.

4.3.3. Phage breakthrough under flow interruption

Figure 4-8 shows the total phage detection and protein recovery from post buffer flush of 50 L/m^2. The main reason of post buffer flush is for recovery of protein loss during virus filtration (LaCasse et al., 2016). In this study, three different phage titers of 10^4, 10^7, and 10^8 PFU/mL were challenged in prior to post buffer flush with 20 g/L BSA co-mixed solution condition, total phage challenge of 3.0 x 10^9, 3.9 x 10^{12} and 2.8 x 10^{13} PFU/m^2. The results clearly showed that increased total phage detection during post buffer flush as phage challenged in membrane increased, while no visible phage detection occurred under 10^4 PFU/mL filtration. Note that the phage detections were mostly occurred in the initial 3 mL of the permeate sample, equivalent to ~10 L/m^2 of buffer flush, then the phage titer was rapidly decreased through rest of buffer flush. Similar trend was observed recently (Afzal & Zydney, 2022), by using single layer of homogeneous Pegasus™ SV4 membrane. The most phage detection of initial stage of buffer flush proved the mobilization of phage via flow interruption, caused migration through membrane, then phage re-constriction via convective buffer flush force. The BSA via pure buffer flush was also detected, from remained filtrate sample near device exit and unexpectedly deposited protein transmission via buffer flush. The noticeable BSA detection occurred up to ~10 L/m^2 of buffer flush sample, where significant titer of phage detected. The results indicated that post buffer flush can recover the possible product loss from virus filtration, but the undesired virus breakthrough could occur at the same time.

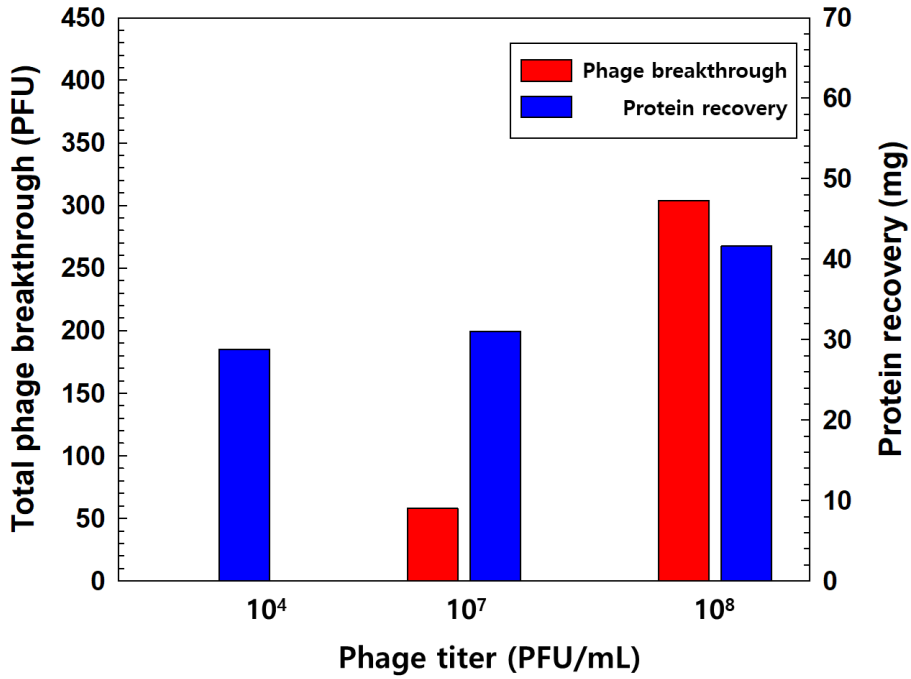

Figure 4-8. Total phage passage (red) and protein recovery (blue) during post buffer flush of 10^4, 10^7, and 10^8 PFU/mL filtration with 20 g/L BSA in 10 mM PBS solution. For post buffer flush, pure PBS solution was used up to 50 L/m^2.

4.3.4. Virus breakthrough behaviors under low filtrate flux

In this section, low flux filtration was investigated to reveal effect of increase diffusive force on phage breakthrough. **Figure 4-9** presented the phage breakthrough profile under 10 LMH filtration for up to 50 L/m^2 filtration under phage titer of 10^4 and 10^7 PFU/mL. The diffusion dominated by Brownian motion can be determined by using the Peclet number as expressed following equation:

$$Pe = \frac{ud}{D} \quad (4\text{-}2)$$

where Pe is the peclet number, u is the solution flow velocity, d is the virus particle diameter and D is the diffusion coefficient of virus particle. Assumed d of 25 - 28 nm (Tars et al., 2000) and the effective diffusion coefficient is estimated as two orders of magnitude lower than free diffusion coefficient, by using following Stokes-Einstein equation (Fan et al., 2021; Yamamoto et al., 2014).

$$D = \frac{k_B T}{3\pi\eta d} \quad (4\text{-}3)$$

where k_B is the Boltzmann constant, T is the absolute temperature of feed solution, η is the dynamic viscosity of feed solution. Based on the previously stated assumptions, Pe = 1 was determined when critical flow velocity range of 21 - 25 LMH by calculated diffusion coefficient for PP7 bacteriophage was 1.45 – 1.74 x 10^{-13} m^2/sec. Therefore, the constant flux of 10 LMH was assumed to be virus diffusive force dominant flow condition. As seen in **Figure 4-9**, the phage breakthrough observed in 10 L/m^2 and the LRV decreased as function of volumetric throughput. The phage breakthrough behavior was completely differed to the connective force dominant flow condition, no phage detected in filtrate up to 300 L/m^2 under the same feed solution condition. However, the 10 LMH filtration of 10^7 PFU/mL PP7 phage with 20 g/L BSA showed similar LRV profile as phage

only condition, indicated the effect of protein presence was not significant as convective force dominant condition by low filtrate flux. Note that under 10^4 PFU/mL filtration with low filtrate flux showed no phage detected in conditions of phage only and phage with 20 g/L BSA, demonstrated safe virus removal performance up to 6 h operation.

To clearly investigate the effect of virus diffusion on virus breakthrough, filtrate flux was switched from convective flow to diffusive flow, for every 50 L/m^2 for 3 cycles (total throughput of 300 L/m^2)., as seen in **Figure 4-10**. Since the low filtrate flux operation was performed under constant flow rate mode, the different flow distribution on membrane possibly caused virus breakthrough, not by the low filtrate flux itself. The effect of different shear stress on protein transmission is reported (Billups et al., 2021); however the effect of shear stress on virus retention behavior was not fully understood. Therefore, the flux switching test was performed under constant pressure operation, with pressure switching was occurred by minimize effect of flow interruption (flow pause less than 1 min). As results, the noticeable LRV change only occurred at low flux of 10 LMH (applied pressure of 0.03 bar). The phage titer in filtrate samples increased by each cycle, indicated that the phage challenged in membrane was responsible for phage breakthrough increase. Based on the results, it is concluded that virus breakthrough under low filtrate flux was mostly by diffusive flow itself, with higher phage challenged caused more severe breakthrough.

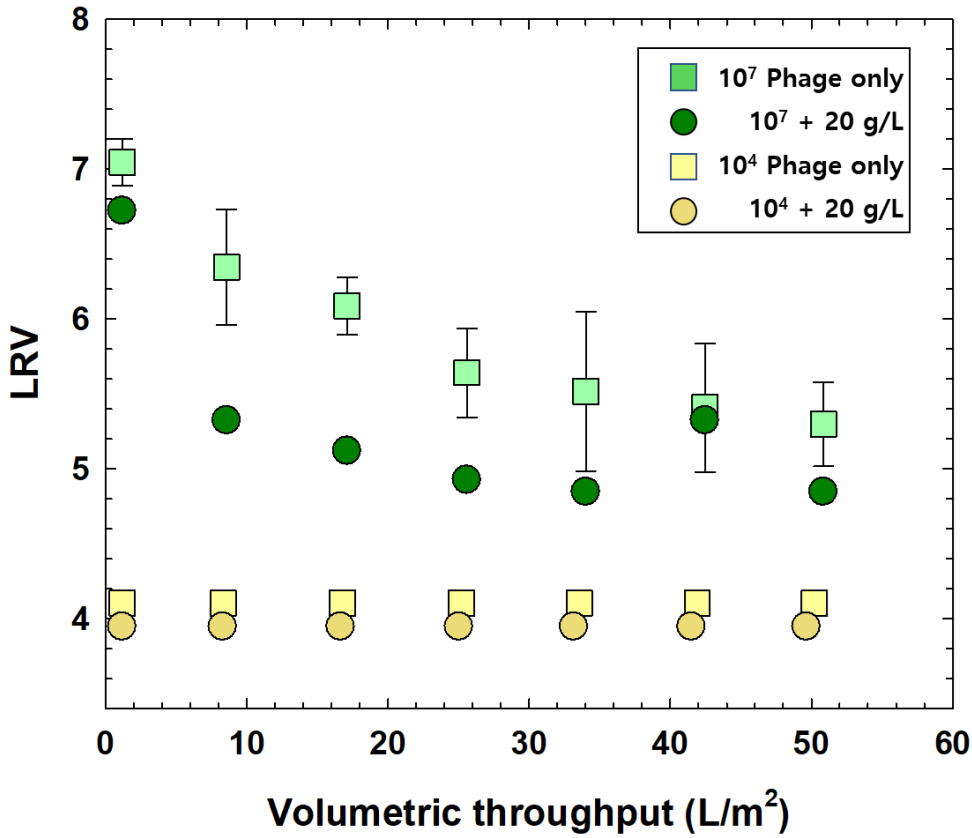

Figure 4-9. LRV as function of volumetric throughput under low flux filtration, 10 LMH, 10^4 and 10^7 PFU/mL of PP7 only and the same phage titers with 20 g/L BSA in 10 mM PBS solution.

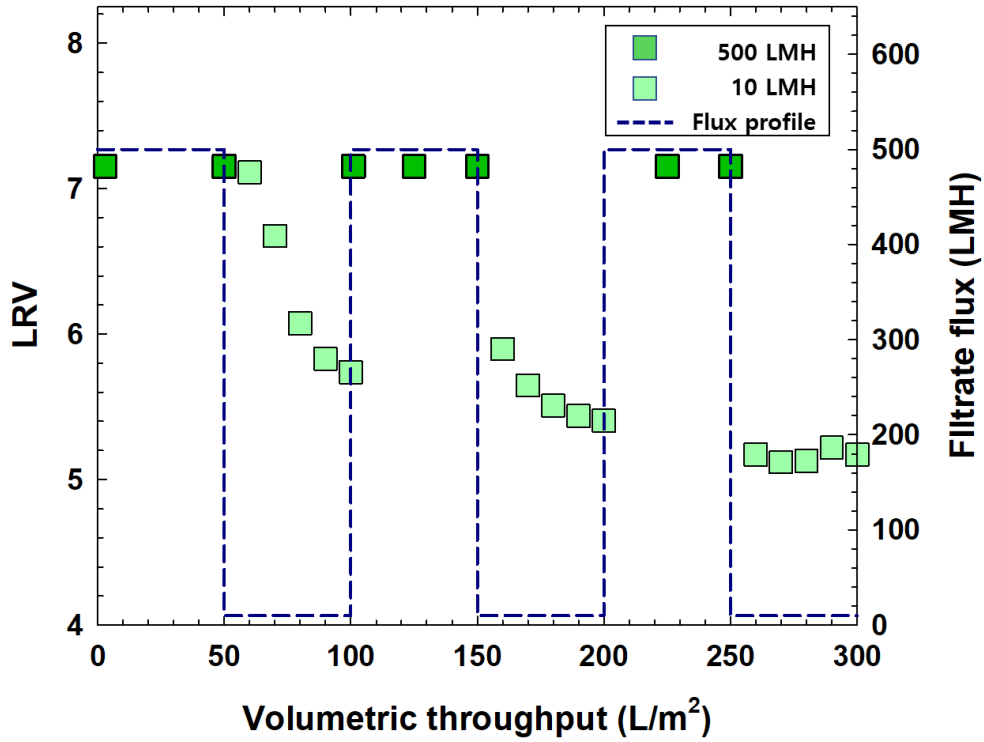

Figure 4-10. LRV as function of volumetric throughput of flux switching test with 10^7 PFU/mL PP7 in 10 mM PBS solution.

4.4. Summary

In this study, the virus breakthrough phenomenon under various operating conditions were investigated by using highly asymmetric virus filtration membrane with using bacteriophage PP7 as virus surrogate. Under conventional filtration condition, phage challenged in membrane over 10^{13} PFU/m^2 showed significant phage passage through membrane. The high titer of PP7 and over 10 g/L BSA co-mixed solution conditions caused increased phage breakthrough over 10-folds higher titer of phage detected in filtrate sample. The flow interruption of 10 min caused undesired migration of virus by increased the Brownian motion, mostly passed the membrane in the initial stage of re-pressurization. Similarly, low flux of 10 LMH constant flow rate operation caused severe virus breakthrough with phage challenge of only 10^{11} PFU/m^2, indicated the potential risk of viral safety in continuous downstream process, where low filtrate flux virus filtration is necessary.

5. Conclusion

In this dissertation, the two major limitations of virus filtration in biopharmaceutical downstream process, protein fouling and virus breakthrough phenomena in practical aspects.

First, the effect of protein fouling and its relationship with virus breakthrough were investigated by using seven different commercial virus filtration membranes. The varied membrane performances of each virus filtration membrane were correlated with structural and surface properties such as membrane symmetricity, pore size gradients, nominal pore size and oxygen content on membrane surface. Higher membrane permeability was shown as membrane structure was highly asymmetric, related to the higher degree of protein fouling propensity than relatively symmetric membranes. Among asymmetric structure membranes, pore size gradients difference of 16 nm/μm caused drastic flux decline compared to pore size gradients of 8 nm/μm membranes. Not only structural properties, but also higher oxygen content on membrane surface showed lower protein fouling propensity. In terms of virus breakthrough, nominal pore size over 23.4 nm with broad pore size distribution showed significant model virus breakthrough, although the virus removal performance was particle and nominal pore size sensitive.

Second part of the dissertation was focused on defining virus breakthrough conditions under various operational conditions, such as high viral loading, sudden flow interruptions and low filtrate flux operations. The virus filtration membrane used in this study successfully retained over 10^6 PFU/mL of model virus surrogate up to 300 L/m^2 of volumetric throughput, proved the robust virus removal performance. However, virus challenged over 10^{13} PFU/m^2 caused unexpected

virus breakthrough, and the presence of protein increased phage passage over one order of magnitude. Under sudden flow interruption or diffusive force dominant flow conditions, virus breakthrough behavior was diffed from conventional virus filtration process, where significant breakthrough observed with lower virus loading of 10^{11} PFU/m^2, but the presence of protein showed minimal impact on virus breakthrough.

The main results of this dissertation give insights to both virus filtration membrane developers and membrane users in downstream process by revealing important structural and surface properties to mitigate protein fouling effect, as well as defining different virus breakthrough points under various feed solution and operating conditions.

6. References

Adams, M. H. (1959). *Bacteriophages*. Interscience Publishers.

Adan-Kubo, J., Tsujikawa, M., Takahashi, K., Hongo-Hirasaki, T., & Sakai, K. (2019). Microscopic visualization of virus removal by dedicated filters used in biopharmaceutical processing: Impact of membrane structure and localization of captured virus particles. *Biotechnology Progress*, *35*(6), 1–11. https://doi.org/10.1002/btpr.2875

Afzal, M. A., & Zydney, A. L. (2022). Effect of filtrate flux and process disruptions on virus retention by a relatively homogeneous virus removal membrane. *Biotechnology Progress*, *38*(4), 5–7. https://doi.org/10.1002/btpr.3255

Ahmed Bouzidi. (2021). Driving biopharma innovation post COVID-10. *European Pharmaceutical Review*.

Ajayi, O. O., Johnson, S. A., Faison, T., Azer, N., Cullinan, J. L., Dement-Brown, J., & Lute, S. C. (2022). An updated analysis of viral clearance unit operations for biotechnology manufacturing. *Current Research in Biotechnology*, *4*, 190–202. https://doi.org/https://doi.org/10.1016/j.crbiot.2022.03.002

Ajayi, O. O., Johnson, S. A., Faison, T., Azer, N., Jackie, L., Dement-brown, J., & Lute, S. C. (2022). An updated analysis of viral clearance unit operations for biotechnology manufacturing. *CURRENT RESEARCH IN BIOTECHNOLOGY*. https://doi.org/10.1016/j.crbiot.2022.03.002

Arkhangelsky, E., & Gitis, V. (2008). Effect of transmembrane pressure on rejection of viruses by ultrafiltration membranes. *Separation and Purification Technology*, *62*(3), 619–628. https://doi.org/10.1016/j.seppur.2008.03.013

Asper, M. (2011). Virus breakthrough after pressure release during virus retentive

filtration. *Parenteral Drug Association Virus and TSE Safety Forum*.

Bakhshayeshi, M., Jackson, N., Kuriyel, R., Mehta, A., van Reis, R., & Zydney, A. L. (2011). Use of confocal scanning laser microscopy to study virus retention during virus filtration. *Journal of Membrane Science*, *379*(1–2), 260–267. https://doi.org/10.1016/j.memsci.2011.05.069

Bakhshayeshi, M., Kanani, D. M., Mehta, A., van Reis, R., Kuriyel, R., Jackson, N., & Zydney, A. L. (2011). Dextran sieving test for characterization of virus filtration membranes. *Journal of Membrane Science*, *379*(1–2), 239–248. https://doi.org/10.1016/j.memsci.2011.05.067

Barnard, J. G., Kahn, D., Cetlin, D., Randolph, T. W., & Carpenter, J. F. (2014). Investigations into the fouling mechanism of parvovirus filters during filtration of freeze-thawed mAb drug substance solutions. *Journal of Pharmaceutical Sciences*, *103*(3), 890–899. https://doi.org/10.1002/jps.23881

Barone, P. W., Wiebe, M. E., Leung, J. C., Hussein, I. T. M., Keumurian, F. J., Bouressa, J., Brussel, A., Chen, D., Chong, M., Dehghani, H., Gerentes, L., Gilbert, J., Gold, D., Kiss, R., Kreil, T. R., Labatut, R., Li, Y., Müllberg, J., Mallet, L., … Springs, S. L. (2020). Viral contamination in biologic manufacture and implications for emerging therapies. *Nature Biotechnology*, *38*(5), 563–572. https://doi.org/10.1038/s41587-020-0507-2

Billups, M., Minervini, M., Holstein, M., Feroz, H., Ranjan, S., Hung, J., Bao, H., Ghose, S., Li, Z. J., & Zydney, A. L. (2021). Antibody retention by virus filtration membranes: Polarization and sieving effects. *Journal of Membrane Science*, *620*(November 2020), 118884. https://doi.org/10.1016/j.memsci.2020.118884

Bohonak, D. M., & Zydney, A. L. (2005). Compaction and permeability effects with virus filtration membranes. *Journal of Membrane Science*, *254*(1–2), 71–79.

https://doi.org/10.1016/j.memsci.2004.12.035

Bolton, G., Cabatingan, M., Rubino, M., Lute, S., Brorson, K., & Bailey, M. (2005). Normal-flow virus filtration: detection and assessment of the endpoint in bioprocessing. *Biotechnology and Applied Biochemistry*, *42*(2), 133. https://doi.org/10.1042/ba20050056

Bolton, G., LaCasse, D., & Kuriyel, R. (2006). Combined models of membrane fouling: Development and application to microfiltration and ultrafiltration of biological fluids. *Journal of Membrane Science*, *277*(1–2), 75–84. https://doi.org/10.1016/j.memsci.2004.12.053

Brickey, K. P., Zydney, A. L., & Gomez, E. D. (2021). FIB-SEM tomography reveals the nanoscale 3D morphology of virus removal filters. *Journal of Membrane Science*, *640*(April), 119766. https://doi.org/10.1016/j.memsci.2021.119766

Burnouf, T., & Radosevich, M. (2003). Nanofiltration of plasma-derived biopharmaceutical products. *Haemophilia*, *9*(1), 24–37. https://doi.org/10.1046/j.1365-2516.2003.00701.x

Charcosset, C. (2012). *Membrane processes in biotechnology and pharmaceutics*. Elsevier.

David, L., Niklas, J., Budde, B., Lobedann, M., & Schembecker, G. (2019). Continuous viral filtration for the production of monoclonal antibodies. *Chemical Engineering Research and Design*, *152*, 336–347. https://doi.org/10.1016/j.cherd.2019.09.040

Dishari, S. K., Micklin, M. R., Sung, K. J., Zydney, A. L., Venkiteshwaran, A., & Earley, J. N. (2015). Effects of solution conditions on virus retention by the Viresolve® NFP filter. *Biotechnology Progress*, *31*(5), 1280–1286.

https://doi.org/10.1002/btpr.2125

Dishari, S. K., Venkiteshwaran, A., & Zydney, A. L. (2015). Probing effects of pressure release on virus capture during virus filtration using confocal microscopy. *Biotechnology and Bioengineering*, *112*(10), 2115–2122. https://doi.org/10.1002/bit.25614

Esfandiary, R., Hayes, D. B., Parupudi, A., Casas-Finet, J., Bai, S., Samra, H. S., Shah, A. U., & Sathish, H. A. (2013). A systematic multitechnique approach for detection and characterization of reversible self-association during formulation development of therapeutic antibodies. *Journal of Pharmaceutical Sciences*, *102*(9), 3089–3099. https://doi.org/10.1002/jps.23654

Fallahianbijan, F., Giglia, S., Carbrello, C., Bell, D., & Zydney, A. L. (2019). Impact of protein fouling on nanoparticle capture within the Viresolve® Pro and Viresolve® NFP virus removal membranes. *Biotechnology and Bioengineering*, *116*(9), 2285–2291. https://doi.org/10.1002/bit.27017

Fallahianbijan, F., Giglia, S., Carbrello, C., & Zydney, A. L. (2017). Use of fluorescently-labeled nanoparticles to study pore morphology and virus capture in virus filtration membranes. *Journal of Membrane Science*, *536*(April), 52–58. https://doi.org/10.1016/j.memsci.2017.04.066

Fallahianbijan, F., Giglia, S., Carbrello, C., & Zydney, A. L. (2020). Quantitative analysis of internal flow distribution and pore interconnectivity within asymmetric virus filtration membranes. *Journal of Membrane Science*, *595*(August 2019), 117578. https://doi.org/10.1016/j.memsci.2019.117578

Fan, R., Namila, F., Sansongko, D., Wickramasinghe, S. R., Jin, M., Kanani, D., & Qian, X. (2021). The effects of flux on the clearance of minute virus of mice during constant flux virus filtration. *Biotechnology and Bioengineering*, *118*(9), 3511–

3521. https://doi.org/10.1002/bit.27778

Gefroh, E., Dehghani, H., McClure, M., Connell-Crowley, L., & Vedantham, G. (2014). Use of MMV as a single worst-case model virus in viral filter validation studies. *PDA Journal of Pharmaceutical Science and Technology*, *68*(3), 297–311. https://doi.org/10.5731/pdajpst.2014.00978

Gerba, C. P. (1984). Applied and Theoretical Aspects of Virus Adsorption to Surfaces. In *Advances in Applied Microbiology* (Vol. 30, Issue C). https://doi.org/10.1016/S0065-2164(08)70054-6

Giglia, S., Bohonak, D., Greenhalgh, P., & Leahy, A. (2015). Measurement of pore size distribution and prediction of membrane filter virus retention using liquid-liquid porometry. *Journal of Membrane Science*, *476*, 399–409. https://doi.org/10.1016/j.memsci.2014.11.053

Goodrich, E. M., Bohonak, D. M., Genest, P. W., & Peterson, E. (2020). *Recent advances in ultra fi ltration and virus fi ltration for production of antibodies and related*. 137–166. https://doi.org/10.1016/B978-0-08-103019-6.00007-2

Guo, W., Ngo, H. H., & Li, J. (2012). A mini-review on membrane fouling. *Bioresource Technology*, *122*, 27–34. https://doi.org/10.1016/j.biortech.2012.04.089

Heffron, J., & Mayer, B. K. (2021). Virus Isoelectric Point Estimation: Theories and Methods. *Applied and Environmental Microbiology*, *87*(3), 1–17. https://doi.org/10.1128/AEM.02319-20

Hermia, J. (1982). *Constant pressure blocking filtration laws: application to power-law non-Newtonian fluids*.

Ho, C.-C., & Zydney, A. L. (2000). A Combined Pore Blockage and Cake Filtration Model for Protein Fouling during Microfiltration. *Journal of Colloid and*

Interface Science, *232*(2), 389–399. https://doi.org/https://doi.org/10.1006/jcis.2000.7231

Hongo-Hirasaki, T., Yamaguchi, K., Yanagida, K., & Okuyama, K. (2006). Removal of small viruses (parvovirus) from IgG solution by virus removal filter Planova®20N. *Journal of Membrane Science*, *278*(1–2), 3–9. https://doi.org/10.1016/j.memsci.2005.10.057

Horowitz, B., Lazo, A., Grossberg, H., Page, G., Lippin, A., & Swan, G. (1998). Virus Inactivation by Solvent/Detergent Treatment and the Manufacture of SD-Plasma. *Vox Sanguinis*, *74*(S1), 203–206. https://doi.org/10.1111/j.1423-0410.1998.tb05473.x

ICH. (2022). *Q5A (R2): Viral safety evaluation of biotechnology products derived from cell lines of human or animal origin. International Conference on Harmonisation of Technical Requirements for Registration of Pharmaceuticals for Human Use*.

Iritani, E., & Katagiri, N. (2016). Developments of blocking filtration model in membrane filtration. *KONA Powder and Particle Journal*, *2016*(33), 179–202. https://doi.org/10.14356/kona.2016024

Jackson, N. B., Bakhshayeshi, M., Zydney, A. L., Mehta, A., van Reis, R., & Kuriyel, R. (2014). Internal virus polarization model for virus retention by the Ultipor® VF Grade DV20 membrane. *Biotechnology Progress*, *30*(4), 856–863. https://doi.org/10.1002/btpr.1897

Johnson, S. A., Chen, S., Bolton, G., Chen, Q., Lute, S., Fisher, J., & Brorson, K. (2022). Virus filtration: A review of current and future practices in bioprocessing. *Biotechnology and Bioengineering*, *119*(3), 743–761. https://doi.org/10.1002/bit.28017

Kern, G., & Krishonan, M. (2006). Virus Removal by Filtration: Points to Consider. *BioPharm International*, *19*(10).

Kosiol, P., Hansmann, B., Ulbricht, M., & Thom, V. (2017). Determination of pore size distributions of virus filtration membranes using gold nanoparticles and their correlation with virus retention. *Journal of Membrane Science*, *533*(January), 289–301. https://doi.org/10.1016/j.memsci.2017.03.043

Kosiol, P., Kahrs, C., Thom, V., Ulbricht, M., & Hansmann, B. (2019). Investigation of virus retention by size exclusion membranes under different flow regimes. *Biotechnology Progress*, *35*(2). https://doi.org/10.1002/btpr.2747

Kosiol, P., Müller, M. T., Schneider, B., Hansmann, B., Thom, V., & Ulbricht, M. (2018). Determination of pore size gradients of virus filtration membranes using gold nanoparticles and their relation to fouling with protein containing feed streams. *Journal of Membrane Science*, *548*(November 2017), 598–608. https://doi.org/10.1016/j.memsci.2017.11.048

LaCasse, D., Lute, S., Fiadeiro, M., Basha, J., Stork, M., Brorson, K., Godavarti, R., & Gallo, C. (2016). Mechanistic failure mode investigation and resolution of parvovirus retentive filters. *Biotechnology Progress*, *32*(4), 959–970. https://doi.org/10.1002/btpr.2298

Ladewig, B., & Al-Shaeli, M. N. Z. (2017). *Fundamentals of Membrane Bioreactors* (Issue October). https://doi.org/10.1007/978-981-10-2014-8

Langlet, J., Ogorzaly, L., Schrotter, J. C., Machinal, C., Gaboriaud, F., Duval, J. F. L., & Gantzer, C. (2009). Efficiency of MS2 phage and Qβ phage removal by membrane filtration in water treatment: Applicability of real-time RT-PCR method. *Journal of Membrane Science*, *326*(1), 111–116. https://doi.org/10.1016/j.memsci.2008.09.044

Leisi, R., Widmer, E., Gooch, B., Roth, N. J., & Ros, C. (2021). Mechanistic insights into flow-dependent virus retention in different nanofilter membranes. *Journal of Membrane Science*, *636*, 119548. https://doi.org/10.1016/j.memsci.2021.119548

Lute, S., Bailey, M., Combs, J., Sukumar, M., & Brorson, K. (2007). Phage passage after extended processing in small-virus-retentive filters. *Biotechnology and Applied Biochemistry*, *47*(3), 141. https://doi.org/10.1042/ba20060254

Marques, B. F., Roush, D. J., & Göklen, K. E. (2009). Virus filtration of high-concentration monoclonal antibody solutions. *Biotechnology Progress*, *25*(2), 483–491. https://doi.org/10.1002/btpr.177

Michen, B., & Graule, T. (2010). Isoelectric points of viruses. *Journal of Applied Microbiology*, *109*(2), 388–397. https://doi.org/10.1111/j.1365-2672.2010.04663.x

Miesegaes, G. (2014). Viral Clearance by Traditional Operations With Significant Knowledge Gaps (Session II): Cation Exchange Chromatography (CEX) and Detergent Inactivation. *PDA Journal of Pharmaceutical Science and Technology*, *68*(1), 30 LP – 37. https://doi.org/10.5731/pdajpst.2014.00964

Miesegaes, G., Lute, S., & Brorson, K. (2010). Analysis of viral clearance unit operations for monoclonal antibodies. *Biotechnology and Bioengineering*, *106*(2), 238–246. https://doi.org/10.1002/bit.22662

Müller, D., Klein, L., Lemke, J., Schulze, M., Kruse, T., Saballus, M., Matuszczyk, J., Kampmann, M., & Zijlstra, G. (2022). Process intensification in the biopharma industry: Improving efficiency of protein manufacturing processes from development to production scale using synergistic approaches. *Chemical Engineering and Processing - Process Intensification*, *171*, 108727. https://doi.org/10.1016/j.cep.2021.108727

Namila, F. N. U., Zhang, D., Traylor, S., Nguyen, T., Singh, N., Wickramasinghe, R., & Qian, X. (2019). The effects of buffer condition on the fouling behavior of MVM virus filtration of an Fc-fusion protein. *Biotechnology and Bioengineering*, *116*(10), 2621–2631. https://doi.org/10.1002/bit.27085

Nazem-Bokaee, H., Chen, D., O'Donnell, S. M., & Zydney, A. L. (2019). New insights into the performance characteristics of the Planova-series hollow-fiber parvovirus filters using confocal and electron microscopy. *Biotechnology and Bioengineering*, *116*(8), 2010–2017. https://doi.org/10.1002/bit.26991

Nejatishahidein, N., & Zydney, A. L. (2021). Depth filtration in bioprocessing — new opportunities for an old technology. *Current Opinion in Chemical Engineering*, *34*(1), 100746. https://doi.org/10.1016/j.coche.2021.100746

Peles, J., Cacace, B., Carbrello, C., Giglia, S., & Zydney, A. L. (2022). Global pore blockage - cake filtration model including pressure effects on protein fouling in virus filtration. *Journal of Membrane Science*, *662*(July), 120961. https://doi.org/10.1016/j.memsci.2022.120961

Peles, J., Fallahianbijan, F., Cacace, B., Carbrello, C., Giglia, S., & Zydney, A. L. (2022). Effect of operating pressure on protein fouling during constant-pressure virus removal filtration. *Journal of Membrane Science*, *648*(February), 120351. https://doi.org/10.1016/j.memsci.2022.120351

Rathore, A. S., Kumar, V., Arora, A., Lute, S., Brorson, K., & Shukla, A. (2014). Mechanistic modeling of viral filtration. *Journal of Membrane Science*, *458*, 96–103. https://doi.org/10.1016/j.memsci.2014.01.037

Roth, N. J., Dichtelmüller, H. O., Fabbrizzi, F., Flechsig, E., Gröner, A., Gustafson, M., Jorquera, J. I., Kreil, T. R., Misztela, D., Moretti, E., Moscardini, M., Poelsler, G., More, J., Roberts, P., Wieser, A., & Gajardo, R. (2020). Nanofiltration as a

robust method contributing to viral safety of plasma-derived therapeutics: 20 years' experience of the plasma protein manufacturers. *Transfusion*, *60*(11), 2661–2674. https://doi.org/10.1111/trf.16022

Russell, K. P., Zydney, A. L., & Gomez, E. D. (2023). Impact of virus filter pore size / morphology on virus retention behavior. *Journal of Membrane Science*, *670*(October 2022), 121335. https://doi.org/10.1016/j.memsci.2022.121335

Shirataki, H., & Wickramasinghe, S. R. (2023). Predicting virus filter performance using an advanced membrane structural model. *Journal of Membrane Science*, *685*(April), 121929. https://doi.org/10.1016/j.memsci.2023.121929

Shirataki, H., Yokoyama, Y., Taniguchi, H., & Azeyanagi, M. (2021). Analysis of filtration behavior using integrated column chromatography followed by virus filtration. *Biotechnology and Bioengineering*, *118*(9), 3569–3580. https://doi.org/10.1002/bit.27840

Shukla, A. A., & Aranha, H. (2015). Viral clearance for biopharmaceutical downstream processes. *Pharmaceutical Bioprocessing*, *3*(2), 127–138. https://doi.org/10.4155/pbp.14.62

Stanevich, V., Pachalla, A., Nunez, B., McInnes, M., Nieder, C., & Schreffler, J. (2021). Improving viral filtration capacity in biomanufacturing processes using aggregate binding properties of polyamide-6,6. *Biotechnology and Bioengineering*, *118*(3), 1105–1115. https://doi.org/10.1002/bit.27634

Strauss, D., Goldstein, J., Hongo-Hirasaki, T., Yokoyama, Y., Hirotomi, N., Miyabayashi, T., & Vacante, D. (2017). Characterizing the impact of pressure on virus filtration processes and establishing design spaces to ensure effective parvovirus removal. *Biotechnology Progress*, *33*(5), 1294–1302. https://doi.org/10.1002/btpr.2506

Suh, D., Kim, M., Lee, C., & Baek, Y. (2022). Virus filtration in biopharmaceutical downstream processes: key factors and current limitations. *Separation & Purification Reviews*, *00*(00), 1–14. https://doi.org/10.1080/15422119.2022.2143379

Syedain, Z. H., Bohonak, D. M., & Zydney, A. L. (2006). Protein fouling of virus filtration membranes: Effects of membrane orientation and operating conditions. *Biotechnology Progress*, *22*(4), 1163–1169. https://doi.org/10.1021/bp050350v

Tars, K., Fridborg, K., Bundule, M., & Liljas, L. (2000). The three-dimensional structure of bacteriophage PP7 from Pseudomonas aeruginosa at 3.7-Å resolution. *Virology*, *272*(2), 331–337. https://doi.org/10.1006/viro.2000.0373

van Reis, R., & Zydney, A. (2007). Bioprocess membrane technology. *Journal of Membrane Science*, *297*(1–2), 16–50. https://doi.org/10.1016/j.memsci.2007.02.045

Van Voorthuizen, E. M., Ashbolt, N. J., & Schäfer, A. I. (2001). Role of hydrophobic and electrostatic interactions for initial enteric virus retention by MF membranes. *Journal of Membrane Science*, *194*(1), 69–79. https://doi.org/10.1016/S0376-7388(01)00522-1

Wälchli, R., Ressurreição, M., Vogg, S., Feidl, F., Angelo, J., Xu, X., Ghose, S., Jian Li, Z., Le Saoût, X., Souquet, J., Broly, H., & Morbidelli, M. (2020). Understanding mAb aggregation during low pH viral inactivation and subsequent neutralization. *Biotechnology and Bioengineering*, *117*(3), 687–700. https://doi.org/10.1002/bit.27237

Wang, W., & Roberts, C. J. (2018). Protein aggregation – Mechanisms, detection, and control. *International Journal of Pharmaceutics*, *550*(1), 251–268. https://doi.org/https://doi.org/10.1016/j.ijpharm.2018.08.043

Wickramasinghe, S. R., Stump, E. D., Grzenia, D. L., Husson, S. M., & Pellegrino, J. (2010). Understanding virus filtration membrane performance. *Journal of Membrane Science*, *365*(1–2), 160–169. https://doi.org/10.1016/j.memsci.2010.09.002

Wieser, A., Modrof, J., & Kreil, T. R. (2023). Protection of biomanufacturing processes from virus contamination through upstream virus filtration of cell culture media. *Biotechnology and Bioengineering*, *April*, 1–8. https://doi.org/10.1002/bit.28473

Woods, M. A., & Zydney, A. L. (2014). Effects of a pressure release on virus retention with the Ultipor DV20 membrane. *Biotechnology and Bioengineering*, *111*(3), 545–551. https://doi.org/10.1002/bit.25112

Yamamoto, A., Hongo-Hirasaki, T., Uchi, Y., Hayashida, H., & Nagoya, F. (2014). Effect of hydrodynamic forces on virus removal capability of Planova™ filters. *AIChE Journal*, *60*(6), 2286–2297. https://doi.org/https://doi.org/10.1002/aic.14392

Zydney, A. L. (2015). Perspectives on integrated continuous bioprocessing - opportunities and challenges. *Current Opinion in Chemical Engineering*, *10*, 8–13. https://doi.org/10.1016/j.coche.2015.07.005

Zydney, A. L. (2016). Continuous downstream processing for high value biological products: A Review. *Biotechnology and Bioengineering*, *113*(3), 465–475. https://doi.org/10.1002/bit.25695

Zydney, A. L. (2021). New developments in membranes for bioprocessing – A review. *Journal of Membrane Science*, *620*(October 2020), 118804. https://doi.org/10.1016/j.memsci.2020.118804

국문 초록

동·식물의 세포주에서 원료를 추출, 정제하여 생산하는 바이오의약품(biopharmaceutical) 제조 산업은 백신, 재조합단백질 및 항체의약품의 수요증가에 따라 전 세계적으로 가파르게 성장하고 있는 산업이다. 바이오의약품 중 동물세포주를 원료로 하는 항체의약품은 제조/정제 과정 중 세포의 바이러스 감염 위험이 있으며, 이는 제품의 안전성 문제를 초래한다. 따라서, 모든 동물세포주를 원료로 하는 항체의약품은 제품의 시판 전 바이러스 안전성 평가를 진행하며, 이는 원재료, 정제공정, 그리고 제품화 순서에 안전성 및 바이러스 제거능력을 검증해야 한다.

대표적인 바이러스 제거 공정으로 고분자 분리막을 사용한 바이러스 필터 공정이 각광받고 있다. 바이러스 필터 공정은 고분자 분리막을 이용하여 size-exclusion메커니즘으로 바이러스를 막 내에서 효과적으로 제거하고 항체의약품은 투과된다. 현재 단일 바이러스 필터 공정으로 약 4-$\log_{10}$ 이상의 바이러스를 제거할 수 있으며 이 때의 제품 투과율은 95% 이상으로 알려져 있다. 현재 바이러스 필터 공정은 단백질 막 오염 현상 (protein fouling)과 바이러스 투과 현상 (virus breakthrough)으로 공정의 한계성을 보여주고 있다. 단백질 막 오염은 바이러스 대신 항체 의약품이 고분자 막 내에 제거가 되어 필터의 성능을 저하시키고, 생산 효율을 감소시킨다. 또한, 바이러스 필터 공정에서 예기치 못한 바이러스의 투과 현상은 제품 안정성에 치명적인 문제를 야기한다. 이러한 공정적 한계점은 최근 downstream 공정의 개발방향인 고농도 의약품 정제 및 연속식 공정에서 더 심각하게 일어나는 것으로 보고되고 있다.

따라서, 본 연구의 목적은 바이러스 필터 공정의 두 한계점에 대한 원인을 파악하고, 이를 개선하는 방안을 바이러스 필터의 제막 디자인 방안과 안정적인 공정 운영점을 설정하여 제시하고자 하였다. 먼저, 7종의 상용 바이러스 필터의 구조적,

표면적 특성을 분석하고 성능과의 연관성을 확인하였다. 비대칭성 구조를 지닌 막들 중에서, 막 표면의 탄소 대비 산소의 함량 (O/C ratio)이 높을수록, 막 상층부의 기공 크기가 크고 하층부의 기공 크기 증감율 (pore size gradient)이 4 – 8 nm/μm 일 때 1 g/L의 소 혈청 알부민의 protein fouling 영향을 66.3% 감소시키는 것으로 나타났다. 또한, 바이러스 제거층의 기공 크기 분포에서 25 nm의 기공이 발견되는 필터에서 예기치 못한 바이러스 투과 현상이 일어나는 것을 확인하여, 고성능 바이러스 필터 제막의 세 가지 중요 인자를 표면 O/C ratio, 막 상층부의의 큰 기공 분포 및 바이러스 제거층의 25nm 미만의 기공크기 분포 및 낮은 기공 크기 증감율로 정의하였다.

두번째로, 고농도 단백질 조건 및 연속성 공정에서의 바이러스 투과 현상을 연구하였다. 그 결과, 상용 바이러스 필터의 바이러스 제거 capacity 가 단위 면적당 약 10^{12} PFU 인 것으로 나타났다. 바이러스가 막의 단위면적당 10^{12} PFU 이상 축적될 시에 바이러스 투과 및 바이러스에 의한 유속 감소 현상이 일어나는 것을 확인하였으며, 20 g/L의 단백질에 의해 바이러스 투과 량이 10배 이상 증가하였다. 또한, 연속 공정운영의 낮은 유속 (10 LMH)의 조건에서 바이러스 확산의 증가로 바이러스 투과현상이 10^{11} PFU/m^{2}의 미만의 축적에도 일어났으며, 이는 유속을 다시 높일 경우 제거능의 회복을 확인하였다. 본 연구의 결과를 바탕으로 바이러스 투과 현상이 일어나지 않는 단위면적당 바이러스 축적 량을 10^{10} PFU/m^{2}로 정의하였으며, 고농도 조건 및 연속 공정에서도 안전한 공정 운영의 가능성을 보여주었다.

본 연구의 결과를 바탕으로, 실제 바이러스 필터 공정에서 일어나는 단백질 막오염 및 바이러스 제거 능력의 변화 예측이 가능할 것으로 보이며, 이에 맞는 공정별 최적화된 바이러스 필터 선정에 기여할 것으로 기대한다. 또한, 제품 안전성을 보증하는 바이러스 필터 공정의 운영의 가이드라인을 제시하여 바이러스 필터 사

용주기 및 제품 안정성을 보장하는 처리수량 혹은 단위면적 설정예측을 효과적으로 할 것으로 보인다. 마지막으로, 차세대 바이러스 분리막을 개발하는 연구계에 바이러스 분리막의 성능을 결정짓는 주유 인자들을 규명함으로써 단백질 막 오염의 영향을 줄이고 높은 바이러스 제거능을 보유하는 차세대 막 개발에 기여할 것으로 예상한다.

주요어: 바이오의약품; 다운스트림 공정; 바이러스 필터; 단백질 막오염; 바이러스 투과

학번: 2014-30293